Investigations of the Influence of Two Pyridyl-Mesoionic Carbene Constitutional Isomers on the Electrochemical and Spectroelectrochemical Properties of Group 6 Metal Carbonyl Complexes

Tobias Bens [1,2] and Biprajit Sarkar [1,2,*]

[1] Institut für Anorganische Chemie, Universität Stuttgart, Pfaffenwaldring 55, 70569, Stuttgart, Germany; tobias.bens@uibk.ac.at
[2] Institut für Chemie und Biochemie, Freie Universität Berlin, Fabeckstraße 34–36, 14195, Berlin, Germany
* Correspondence: biprajit.sarkar@iac.uni-stuttgart.de

Keywords: mesoionic carbenes; (spectro)electrochemistry; carbonyl ligands; group 6 carbonyls; EPR spectroscopy

S1. Experimental Section 4

S1.10 General Procedures, Materials and Instrumentation 4

S1.30 Electrochemistry 5

S1.40 Spectroelectrochemistry 5

S1.50 DFT 6

S2. Cyclic Voltammetry 8

S2.10 Cyclic Voltammetry of [Cr(**C–C**)$(CO)_4$] 8

S2.20 Cyclic Voltammetry of [Cr(**C–N**)$(CO)_4$] 9

S2.30 Cyclic Voltammetry of [Mo(**C–C**)$(CO)_4$] 10

S2.40 Cyclic Voltammetry of [Mo(**C–N**)$(CO)_4$] 12

S2.50 Cyclic Voltammetry of [W(**C–C**)$(CO)_4$] 12

S2.60 Cyclic Voltammetry of [W(**C–N**)$(CO)_4$] 13

S3. Spin Density Calculations 14

S4. IR-Spectroelectrochemistry and DFT Calculations 14

S4.10 IR-Spectroelectrochemistry of [Cr(**C–C**)$(CO)_4$] 14

S4.11 Calculated IR Spectra of [Cr(**C–C**)$(CO)_4$] and [Cr(**C–C**)$(CO)_4]^-$ 16

S4.20 IR-Spectroelectrochemistry of [Mo(**C–C**)$(CO)_4$] 17

S4.21 Calculated IR Spectra of [Mo(**C–C**)$(CO)_4$] and [Mo(**C–C**)$(CO)_4]^-$ 18

S4.30 IR-Spectroelectrochemistry of [W(**C–C**)$(CO)_4$] 19

S4.31 Calculated IR Spectra of [W(**C–C**)$(CO)_4$] and [W(**C–C**)$(CO)_4]^-$ 20

S4.40 IR-Spectroelectrochemistry of [W(**C–N**)$(CO)_4$] 21

S4.41 Calculated IR Spectra of [W(**C–N**)$(CO)_4$] and [W(**C–N**)$(CO)_4]^-$ 22

S5. UV/vis/NIR-Spectroelectrochemistry 23

S5.10 UV/vis/NIR-Spectroelectrochemistry of [Cr(**C–C**)$(CO)_4$] 23

S5.20 UV/vis/NIR-Spectroelectrochemistry of [Mo(**C–C**)] 23

S5.30 UV/vis/NIR-Spectroelectrochemistry of [W(**C–C**)$(CO)_4$] 24

S5.40 UV/vis/NIR-Spectroelectrochemistry of [W(**C–N**)$(CO)_4$] 24

S6. TD-DFT Calculations 25

S6.10 TD-DFT Calculations of [Cr(**C–C**)$(CO)_4]^-$ 25

S6.20 TD-DFT Calculations of [Mo(**C–C**)$(CO)_4$] and [Mo(**C–C**)$(CO)_4]^-$ 30

S6.30 TD-DFT Calculations of [W(**C–C**)$(CO)_4$] and [W(**C–C**)$(CO)_4]^-$ 39

S6.40 TD-DFT Calculations of [W(**C–N**)(CO)$_4$] and [W(**C–N**)(CO)$_4$]$^-$ 49

S7. Electrochemical CO_2 Reduction 58

S7.10 Electrochemical CO_2 Reduction with [Cr(**C–C**)(CO)$_4$] 58

S7.20 Electrochemical CO_2 Reduction with [Cr(**C–N**)(CO)$_4$] 59

S7.30 Electrochemical CO_2 Reduction with [Mo(**C–C**)(CO)$_4$] 60

S7.40 Electrochemical CO_2 Reduction with [Mo(**C–N**)(CO)$_4$] 61

S1. Experimental Section

S1.10 General Procedures, Materials and Instrumentation

Caution! *Compounds containing azides are potentially explosive. Although we never experienced any problems during synthesis or analysis, all compounds should be synthesized only in small quantities and handled with great care!*

Unless otherwise noted, all reactions were carried out using standard Schlenk-line-techniques under an inert atmosphere of argon (Linde Argon 4.8, purity 99.998%) or in a glovebox (Glovebox Systemtechnik, GS095218).

Commercially available chemicals were used without further purification. The solvents used for metal complex synthesis and catalysis were available from MBRAUN MB-SPS-800 solvent System and degassed by standard techniques prior to use. The identity and purity of compounds were established *via* ^{1}H and ^{13}C NMR spectroscopy, elemental analysis and mass spectrometry.

Solvents for cyclic voltammetry and UV/vis- and EPR-spectroelectrochemical measurements were dried and distilled under argon and degassed by common techniques prior to use. Column chromatography was performed over silica 60 M (0.04 – 0.063 mm).

^{1}H and ^{13}C{^{1}H} NMR spectra were recorded on a Bruker Avance 400 spectrometer at 19 – 22 °C. Chemical shifts are reported in ppm referenced to the residual solvent peaks.[1]

The following abbreviations are used to represent the multiplicity of the signals: s (singlet), d (doublet), t (triplet), q (quartet), p (pentet), sept (septet).

Mass spectrometry was performed on an Agilent 6210 ESI-TOF.

Elemental analyses were performed with an Elementar Micro Cube elemental analyser.

The light-induced syntheses were performed with a LOT-QuantumDesign Arc Lamp (150 W, Xe OF).

[1] S. Budavari (Ed.) *The Merck-index*. *An encyclopedia of chemicals, drugs, and biologicals*, Rahway, NJ, **1991**.

S1.30 Electrochemistry

Cyclic voltammograms were recorded with a PalmSens4 potentiostat or PAR VersaStat (Ametek), respectively, with a conventional three-electrode configuration consisting of a glassy carbon working electrode or gold working electrode, a platinum auxiliary electrode, and a coiled silver wire as a pseudo reference electrode. The (decamethyl)ferrocene/(decamethyl)ferrocenium couple was used as internal reference. All measurements were performed at room temperature with a scan rate between 25 and 1000 mVs^{-1}. The experiments were carried out in absolute Acetonitrile containing 0.1 M Bu_4NPF_6 (Sigma Aldrich, ≥ 99.0%, electrochemical grade) as the supporting electrolyte.

S1.40 Spectroelectrochemistry

UV/vis spectra were recorded with a Avantes spectrometer consisting of a light source (AvaLight-DH-S-Bal), a UV/vis detector (AvaSpec-ULS2048), and an NIR detector (AvaSpec-NIR256-TEC). IR spectra were recorded with a BRUKER Vertex 70 FT-IR or Nicolet 6700 FT-IR spectrometer, respectively. UV/vis-spectroelectrochemical measurements were carried out in an optically transparent thin-layer electrochemical (OTTLE)[2] cell (CaF_2 windows) with a gold-mesh working electrode, a platinum-mesh counter electrode, and a silver-foil pseudo reference. EPR spectra at the X-band frequency (ca. 9.5 GHz) were obtained with a Magnettech MS-5000 benchtop EPR spectrometer equipped with a rectangular TE 102 cavity and a TC HO4 temperature controller. The measurements were carried out in synthetic quartz glass tubes. For EPR spectroelectrochemistry, a three-electrode setup was employed using two Teflon-coated platinum wires (0.005 in. bare and 0.008 in. coated) as the working and counter

electrodes and a Teflon-coated silver wire (0.005 in. bare and 0.007 in coated) as the pseudo reference electrode. The experiments were carried out in absolute Acetonitrile containing 0.1 M Bu_4NPF_6 as the supporting electrolyte. The same solvents as for the CV measurements were used for each compound.

[2] a) J. Klein, A. Stuckmann, S. Sobottka, L. Suntrup, M. van der Meer, P. Hommes, H.-U. Reissig, B. Sarkar, *Chem. Eur. J*. **2017**, *23*, 12314; b) M. Krejčik, M. Daněk, M., F. Hartl, *J. Electroanal. Chem. Interf. Electrochem.* **1991**, *317*, 179.

S1.50 DFT

The program package ORCA 4.1. was used for all DFT calculations.[3] Starting from the molecular structure obtained from X-ray diffraction geometry optimizations were carried out using the B3LYP[4] functional and no symmetry restrictions were imposed during the optimization. For tungsten relativistic effects in zero-order regular approximation (ZORA) were included.[5] All calculations were performed with empirical Van der Waals correction (D3).[6] The restricted and unrestricted DFT methods were employed for closed and open shell molecules respectively unless stated otherwise. Convergence criteria were set to default for geometry-optimization (OPT), and tight for SCF calculations (TIGHTSCF). Triple-ζ–valence basis sets (def2-TZVP)[7] were employed for all atoms. Calculations were performed using resolution of the identity approximation[8] with matching auxiliary basis sets[8] for geometry optimizations and numerical frequency calculations and the RIJCOSX (combination of the resolution of the identity and chain of spheres algorithms) approximation for single point calculations using the B3LYP functional. Low-lying excitation energies were calculated with time-dependent DFT (TD-DFT). Solvent effects were taken into account with the conductor-like polarizable continuum model, CPCM.[9] Spin densities were calculated according to the Mulliken population analysis.[10] The absence of imaginary frequency Spin densities, molecular orbitals and difference densities were visualized with the modified Chemcraft 1.8 program.[11] All molecular orbitals are

illustrated with an iso value of 0.052. All calculated TD-DFT spectra are Gaussian broadened with a band width of 25 at half height unless otherwise noted.

[3] F. Neese, *Wiley Interdiscip. Rev. Comput. Mol. Sci*. **2012**, *2*, 73.

[4] a) S. Grimme, S. Ehrlich, L. Goerigk, *J. Comput. Chem.* **2011**, *32*, 1456; b) S. Grimme, J. Antony, S. Ehrlich, H. Krieg, *J. Chem. Phys*. **2010**, *132*, 154104; c) S. Grimme, *J. Comput. Chem*. **2004**, *25*, 1463; d) S. Grimme, *J. Comput. Chem*. **2006**, *27*, 1787.

[5] van Wüllen, *C. J. Chem. Phys*. **1998**, *109*, 392−399.

[6] a) S. Grimme, S. Ehrlich, L. Goerigk, *J. Comput. Chem.* **2011**, *32*, 1456; b) S. Grimme, J. Antony, S. Ehrlich, H. Krieg, *J. Chem. Phys*. **2010**, *132*, 154104; c) S. Grimme, *J. Comput. Chem*. **2004**, *25*, 1463; d) S. Grimme, *J. Comput. Chem*. **2006**, *27*, 1787.

[7] F. Weigend, R. Ahlrichs, *Phys. Chem. Chem. Phys*. **2005**, *7*, 3297.

[8] a) F. Neese, *J. Comput. Chem*. **2003**, *24*, 1740; b) F. Neese, F. Wenmohs, A. Hansen, U. Becker, *Chem. Phys.* **2009**, *356*, 98; c) O. Vahtras, J. Almloef, M. W. Feyereisen, *Chem. Phys. Lett*. **1993**, *213*, 514; d) J. L. Whitten, *J. Chem. Phys.* **1973**, *58*, 4496; e) R. Izsak; F. Neese, *J. Chem. Phys*. **2011**, *135*, 144105; f) F. Neese, G. Olbrich, *Chem. Phys. Lett*. **2002**, *362*, 170; g) T. Petrenko, S. Kossmann, F. Neese, *J. Chem. Phys.* **2011**, *134*, 054116.

[9] V. Barone, M. Cossi *J. Phys. Chem. A* **1998**, *102*, 1995.

[10] R. S. Mulliken, *J. Chem. Phys*. **1955**, *23*, 1833.

[11] a) M. D. Hanwell, D. E. Curtis, D. C. Lonie, T. Vandermeersch, E. Zurek and G. R. Hutchison, *J. Cheminform*. **2012**, *4*, 17; b) G. A. Zhurko *Chemcraft-Graphical Program for Visualization of Quantum Chemistry Computations*; Chemcraft, Version 1.8: Ivanovo, Russia, 2023, http://www.chemcraftprog.com.

S2. Cyclic Voltammetry

S2.10 Cyclic Voltammetry of [Cr(C–C)(CO)$_4$]

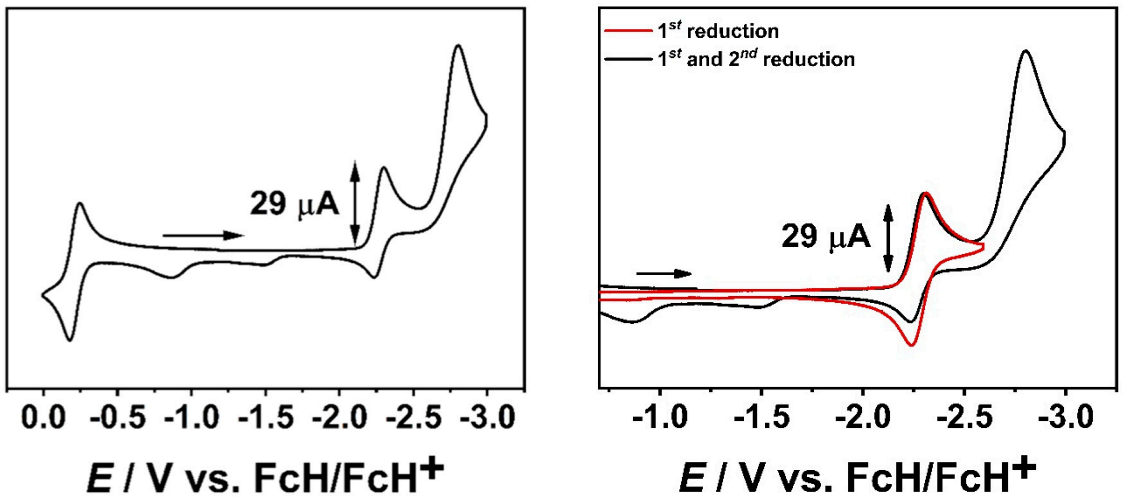

Figure S1. Cyclic voltammograms of [Cr(**C–C**)(CO)$_4$] in CH_3CN and 0.1 M Bu_4NPF_6 at a scan rate of 100 mV/s and a glassy carbon working electrode.

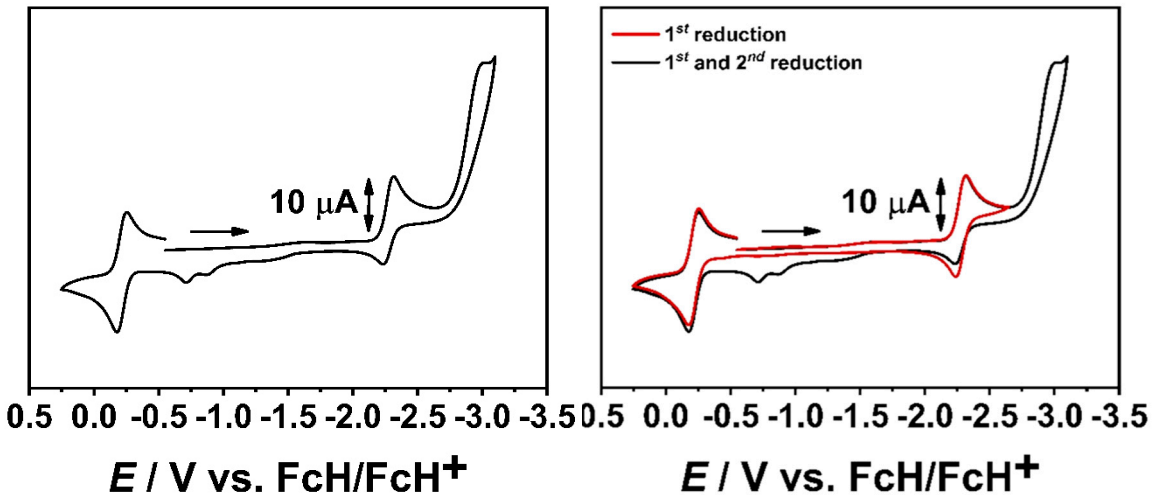

Figure S2. Cyclic voltammograms of [Cr(**C–C**)(CO)$_4$] in CH_3CN and 0.1 M Bu_4NPF_6 at a scan rate of 100 mV/s and a gold working electrode.

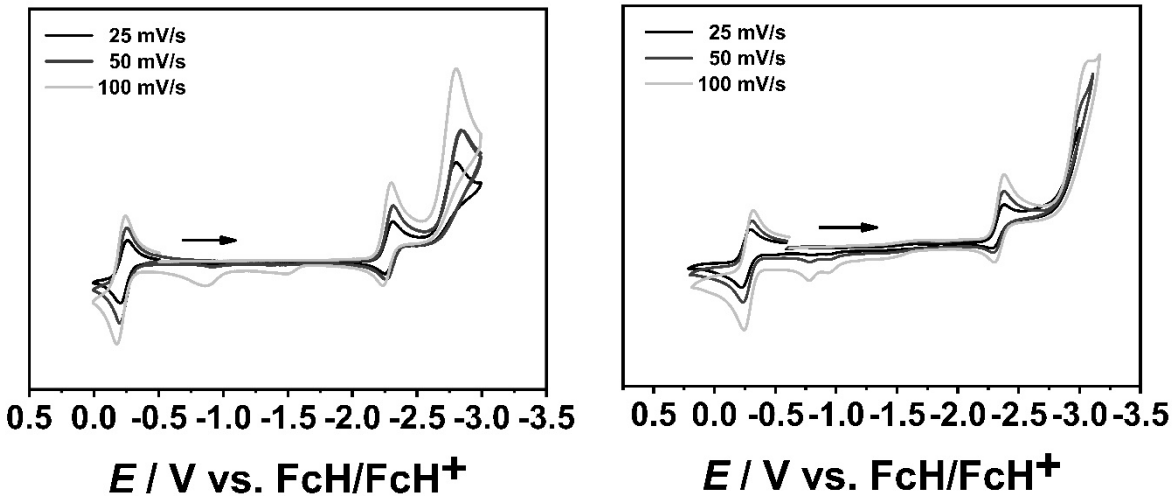

Figure S3. Scan rate dependency in cyclic voltammetry of complex [Cr(**C–C**)(CO)$_4$] in CH_3CN and 0.1 M NBu_4PF_6 (GC: left; Au: right).

S2.20 Cyclic Voltammetry of [Cr(C–N)(CO)$_4$]

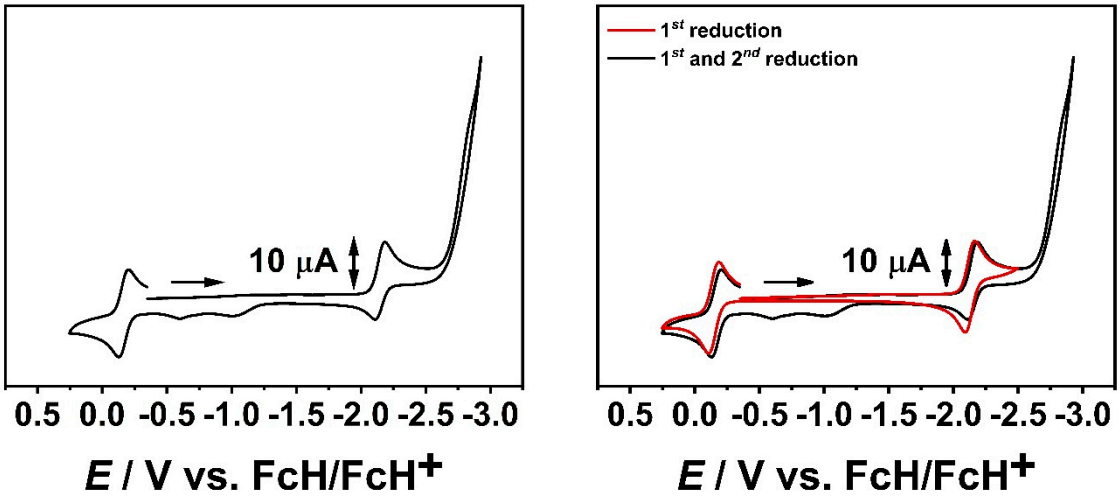

Figure S4. Cyclic voltammograms of [Cr(**C–N**)(CO)$_4$] in CH_3CN and 0.1 M Bu_4NPF_6 with a scan rate of 100 mV/s and a gold working electrode.

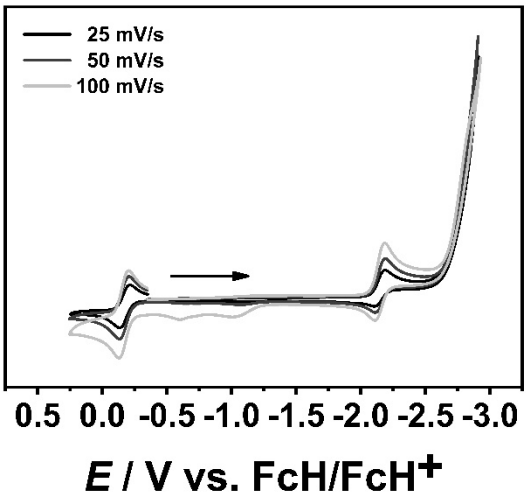

Figure S5. Scan rate dependency in cyclic voltammetry of complex [Cr(**C–N**)(CO)$_4$] in CH_3CN and 0.1 M NBu_4PF_6 and a Au working electrode.

S2.30 Cyclic Voltammetry of [Mo(C–C)(CO)$_4$]

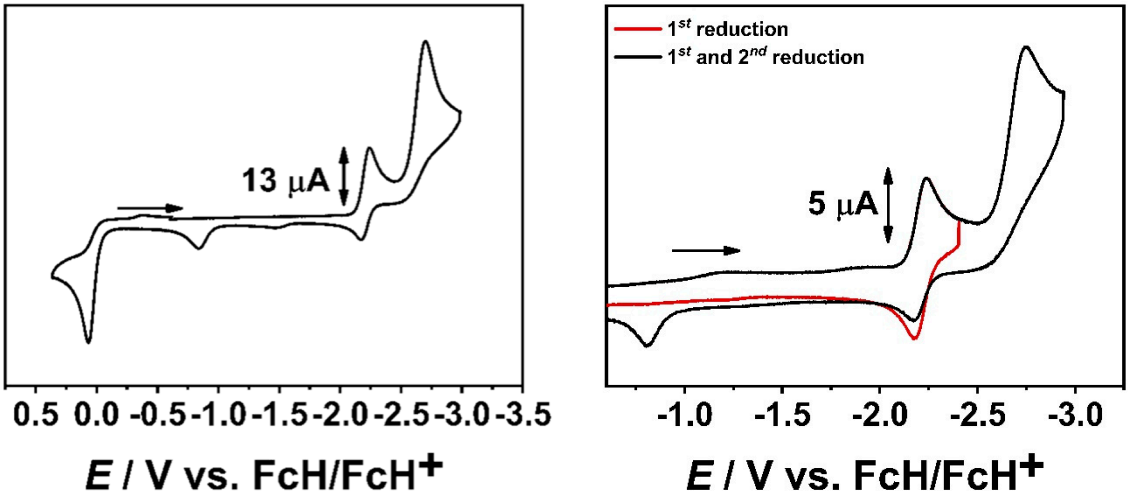

Figure S6. Cyclic voltammograms of [Mo(**C–C**)(CO)$_4$] in CH_3CN and 0.1 M Bu_4NPF_6 at a scan rate of 100 mV/s and a glassy carbon working electrode.

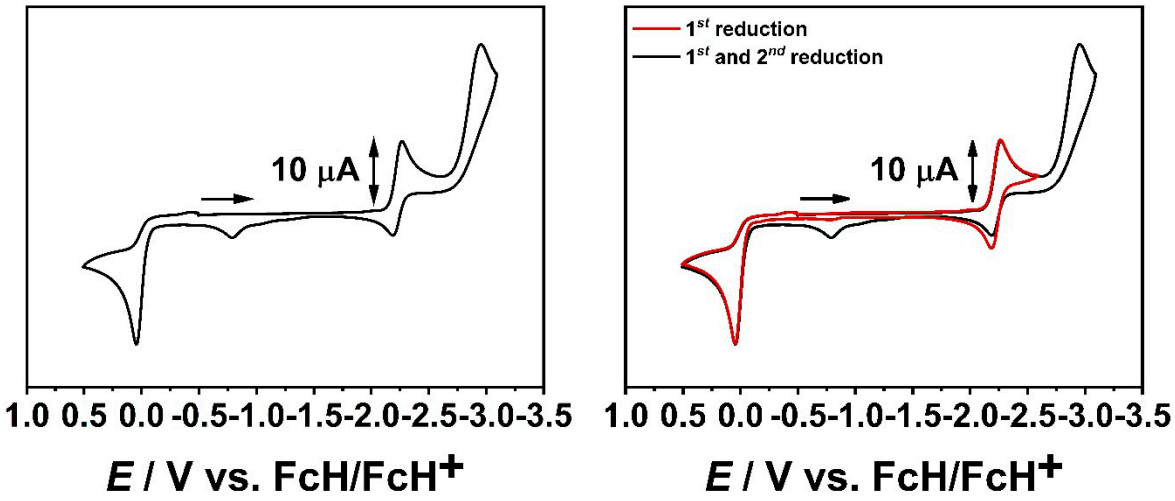

Figure S7. Cyclic voltammograms of [Mo(**C–C**)(CO)$_4$] in CH_3CN and 0.1 M Bu_4NPF_6 at a scan rate of 100 mV/s and a gold working electrode.

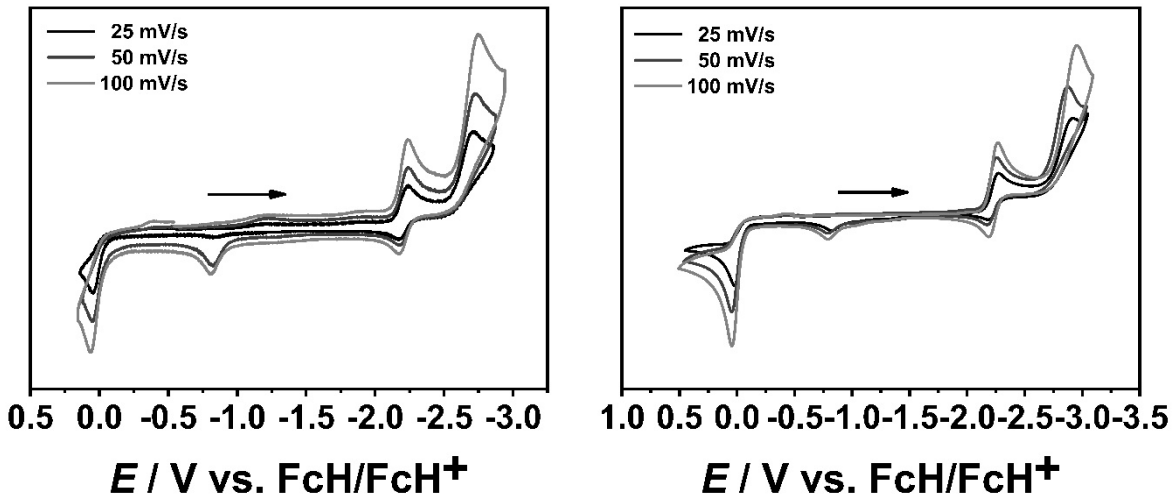

Figure S8. Scan rate dependency in cyclic voltammetry of complex [Mo(**C–C**)(CO)$_4$] in CH_3CN and 0.1 M NBu_4PF_6. (GC: left; Au: right).

S2.40 Cyclic Voltammetry of [Mo(C–N)(CO)$_4$]

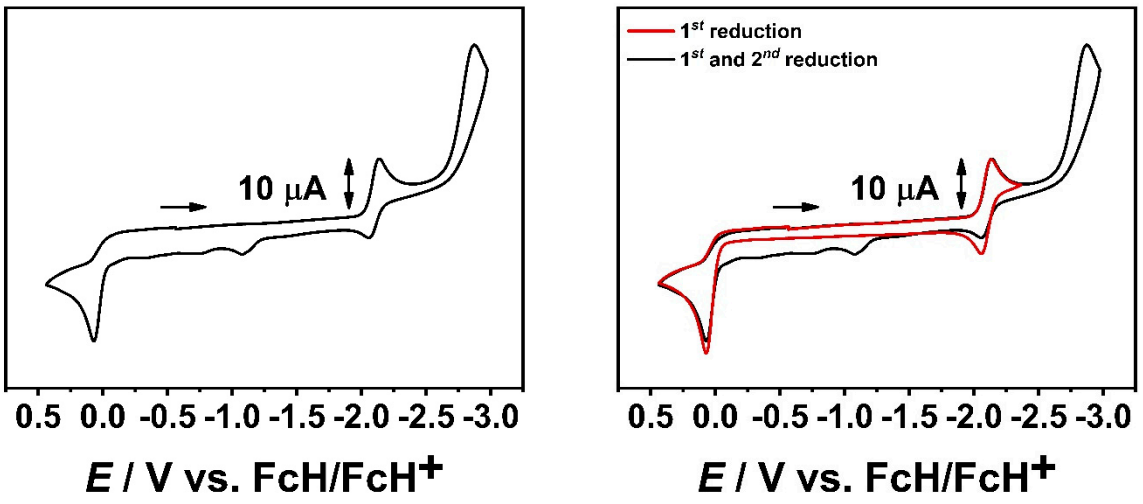

Figure S9. Cyclic voltammograms of [Mo(**C–N**)(CO)$_4$] in CH_3CN and 0.1 M Bu_4NPF_6 at a scan rate of 100 mV/s and a gold working electrode.

S2.50 Cyclic Voltammetry of [W(C–C)(CO)$_4$]

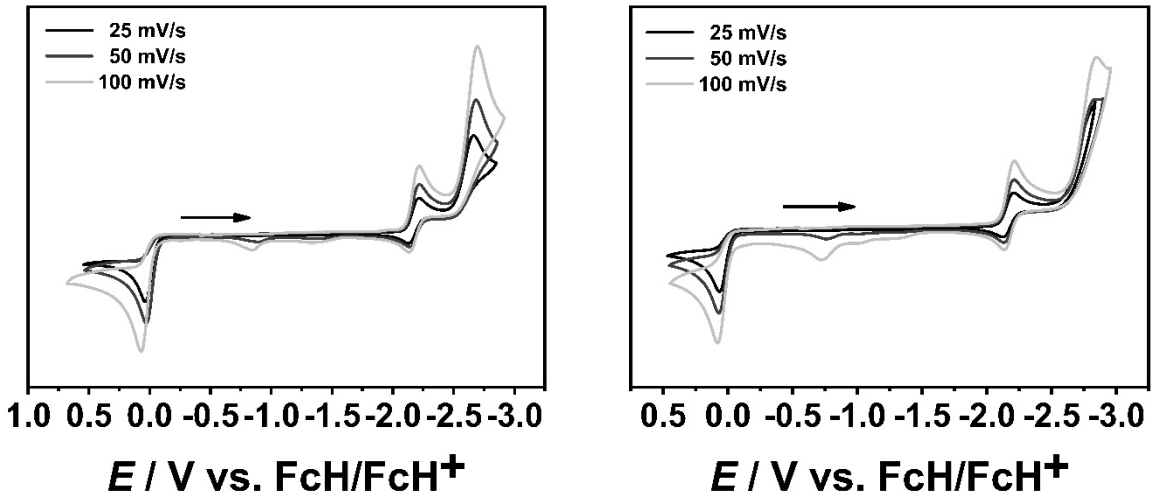

Figure S10. Scan rate dependency in cyclic voltammetry of complex [W(**C–C**)(CO)$_4$] in CH_3CN and 0.1 M NBu_4PF_6. (GC: left; Au: right).

S2.60 Cyclic Voltammetry of [W(C–N)(CO)$_4$]

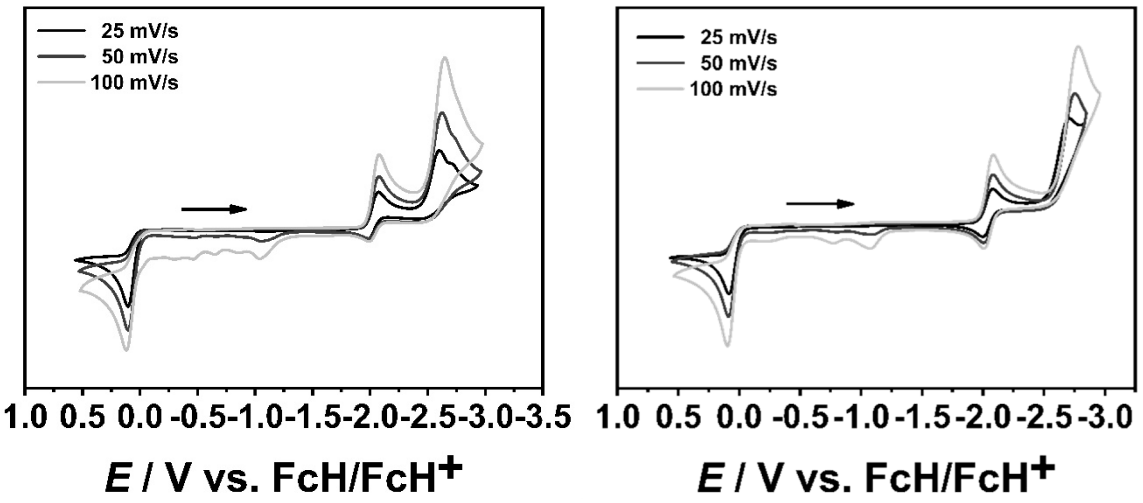

Figure S11. Scan rate dependency in cyclic voltammetry of complex [W(**C–N**)(CO)$_4$] in CH_3CN and 0.1 M NBu_4PF_6. (GC: left; Au: right).

Table S1. Redox potentials of [M(**C–C**)(CO)$_4$]and [M(**C–N**)(CO)$_4$] (M = Cr, Mo, W) in CH_3CN and 0.1 M NBu_4PF_6 at 100 mV/s with a gold working electrode.

	1. Red. / V		**2. Red. / V**	**1. Ox. / V**	
	$E_{1/2}^{red1}$	ΔE_p	E_p^{red2}	$E_{1/2}^{ox1}$	ΔE_p
[Cr(**C–C**)(CO)$_4$]	−2.28	0.08	−3.08	−0.21	0.07
[Cr(**C–N**)(CO)$_4$]	−2.13	0.08	−2.89	−0.16	0.08
[Mo(**C–C**)(CO)$_4$]	−2.22	0.08	−2.96	0.05[a]	
[Mo(**C–N**)(CO)$_4$]	−2.10	0.08	−2.88	0.07[a]	
[W(**C–C**)(CO)$_4$]	−2.19	0.07	−2.85	0.07[a]	
[W(**C–N**)(CO)$_4$]	−2.04	0.08	−2.78	0.10[a]	

[a] $= E_p^{ox}$

S3. Spin Density Calculations

Table S2. Composition of $[M(\mathbf{C–C})(CO)_4]^-$ and $[M(\mathbf{C–N})(CO)_4]^-$ (M = Cr, Mo, W) in Loewdin spin density.

MO	Composition (%)			
	M	**L + | −**	**CO_{ax} + | −**	**CO_{eq} + | −**
$[Cr(C–C)(CO)_4]^-$	−0.8	103.8 | −3.4	0.4 | −0.3	0.3 | 0.0
$[Cr(C–N)(CO)_4]^-$ [12]	−0.4	99.3 | −1.0	0.9 | 0.0	1.2 | 0.0
$[Mo(C–C)(CO)_4]^-$	−0.5	103.0 | −2.7	0.3 | −0.1	0.5 | −0.5
$[Mo(C–N)(CO)_4]^-$ [12]	−0.7	98.5 | −1.0	1.1 | 0.0	2.1 | 0.0
$[W(C–C)(CO)_4]^-$	0.0	100.4 | −0.0	0.0 | 0.0	0.0 | 0.0
$[W(C–N)(CO)_4]^-$	0.0	77.5 | −15.2	0.0 | 0.0	0.0 | 0.0

[12] T. Bens, P. Boden, P. Di Martino-Fumo, J. Beerhues, U. Albold, *S.* Sobottka, *N. I.* Neuman, M. Gerhards, B. Sarkar, *Inorg. Chem.* **2020**, *59*, 15504.

S4. IR-Spectroelectrochemistry and DFT Calculations

S4.10 IR-Spectroelectrochemistry of $[Cr(C–C)(CO)_4]$

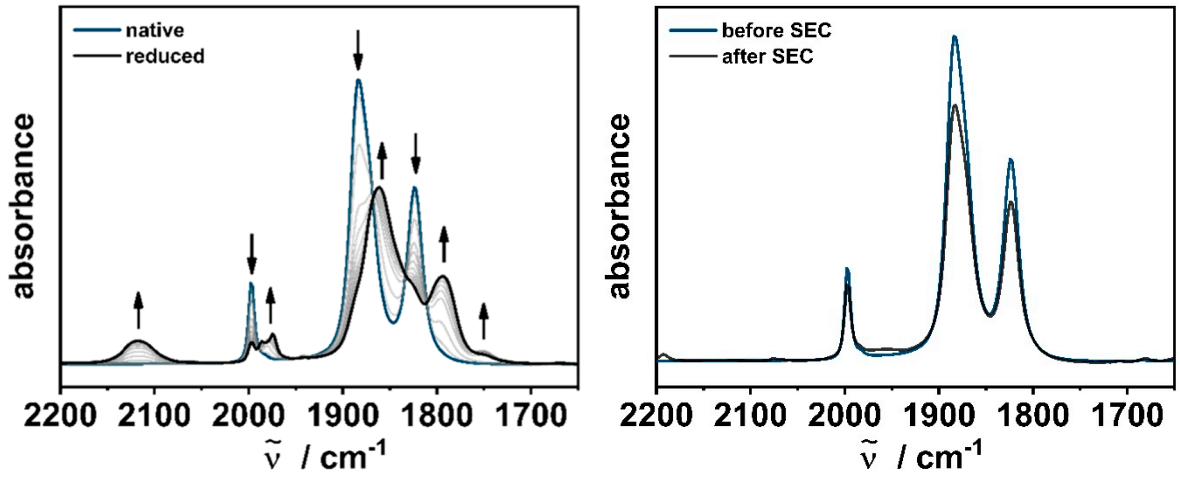

Figure S12. Changes in the IR spectra of $[Cr(\mathbf{C–C})(CO)_4]$ in CH_3CN/0.1 M Bu_4NPF_6 with a Au working electrode during the first reduction (left) and after IR-SEC (right).

Table S3. Experimental and calculated changes (B3LYP/RIJCOSX/D3BJ/def2-TZVP) in the CO frequencies of [Cr(**C–C**)$(CO)_4$] in CH_3CN/0.1 M Bu_4NPF_6 with a Au working electrode during the first reduction.

		$\tilde{\upsilon}$ **(CO) / cm^{-1}**						
exp.	**[Cr(C–C)$(CO)_4$]**	1998	1882	1874 (sh)	1824			
	[Cr(C–C)$(CO)_4$]$^-$	2118[a]	1986	1975	1861	1845 (sh)	1794	1751
calc.	**[Cr(C–C)$(CO)_4$]**	2045	1906	1903	1853			
	[Cr(C–C)$(CO)_4$]$^-$	2029	1884	1876	1820			

[a] free CO

S4.11 Calculated IR Spectra of [Cr(C–C)(CO)$_4$] and [Cr(C–C)(CO)$_4$]$^-$

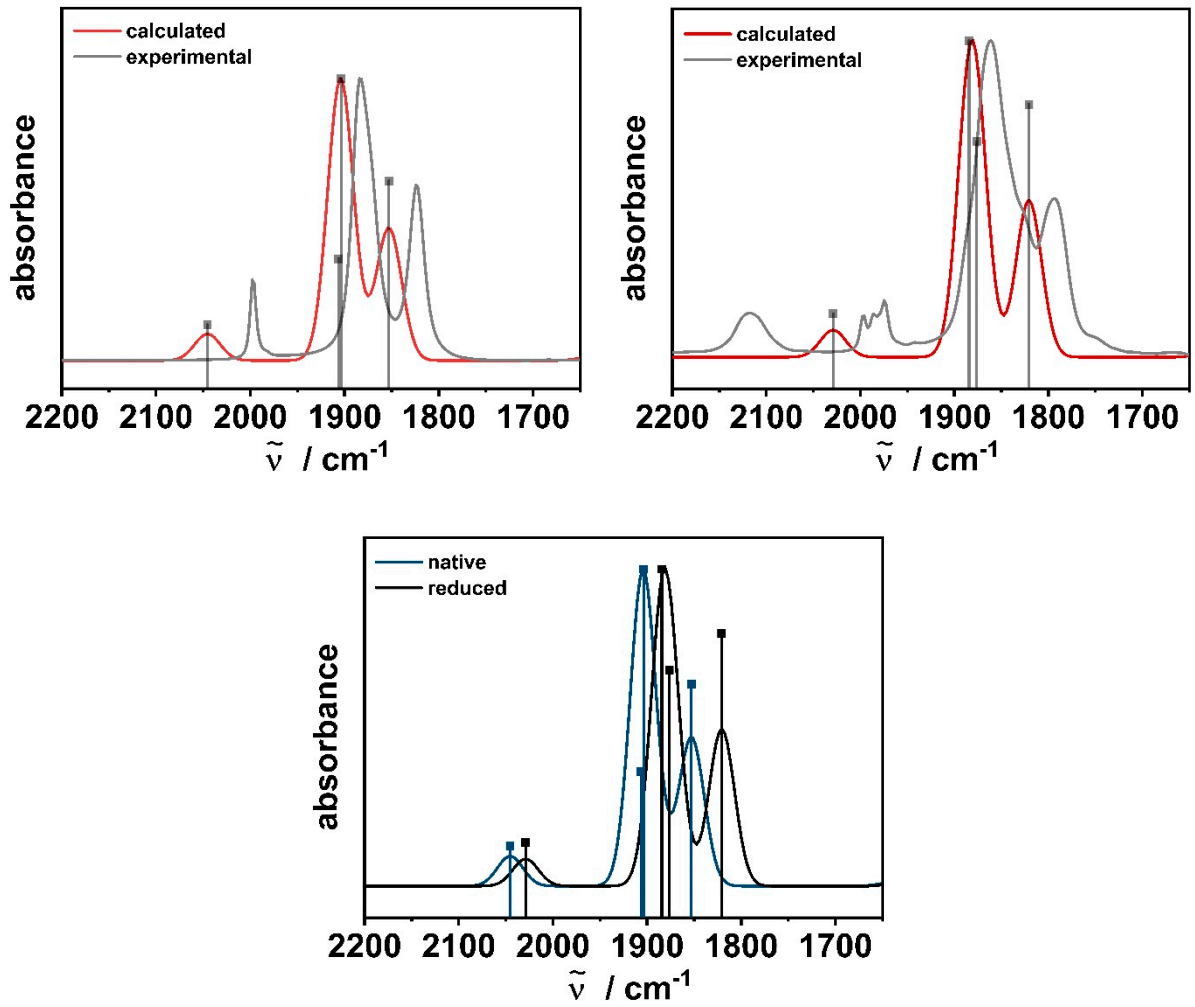

Figure S13. Top left: Calculated (red) and experimental (grey) IR spectra of [Cr(**C–C**)(CO)$_4$], Top right: Calculated (red) and experimental (grey) IR spectra of [Cr(**C–C**)(CO)$_4$]$^-$ and bottom centered: Overlay of calculated [Cr(**C–C**)(CO)$_4$] (blue) and [Cr(**C–C**)(CO)$_4$]$^-$ (black) (B3LYP/RIJCOSX/D3BJ/def2-TZVP, FWHM = 32).

S4.20 IR-Spectroelectrochemistry of [Mo(C–C)(CO)$_4$]

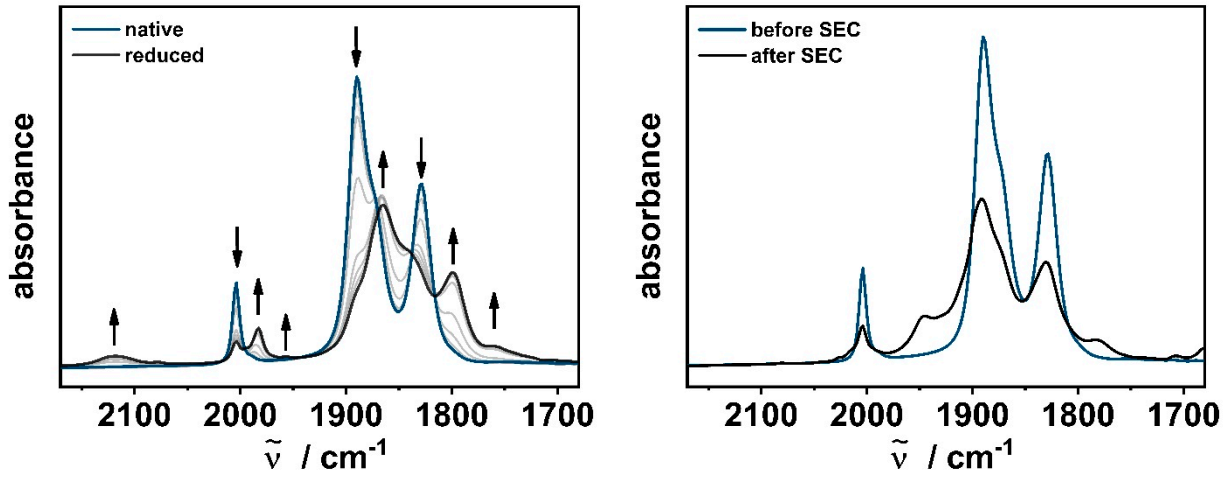

Figure S14. Changes in the IR spectra of [Mo(**C–C**)(CO)$_4$] in CH_3CN/0.1 M Bu_4NPF_6 with a Au working electrode during the first reduction (left) and after IR-SEC (right).

Table S4. Experimental and calculated changes (B3LYP/RIJCOSX/D3BJ/def2-TZVP) in the CO frequencies of [Mo(**C–C**)(CO)$_4$] in CH_3CN/0.1 M Bu_4NPF_6 with a Au working electrode during the first reduction.

		$\tilde{\upsilon}$ **(CO) / cm^{-1}**						
exp.	**[Mo(C–C)(CO)$_4$]**	2004	1890	1876 (sh)	1828			
	[Mo(C–C)(CO)$_4$]$^-$	2119[a]	1982	1957	1865	1842	1799	1759
calc.	**[Mo(C–C)(CO)$_4$]**	2051	1904	1894	1830			
	[Mo(C–C)(CO)$_4$]$^-$	2036	1881	1869	1807			

[a] free CO

S4.21 Calculated IR Spectra of [Mo(C–C)(CO)$_4$] and [Mo(C–C)(CO)$_4$]$^-$

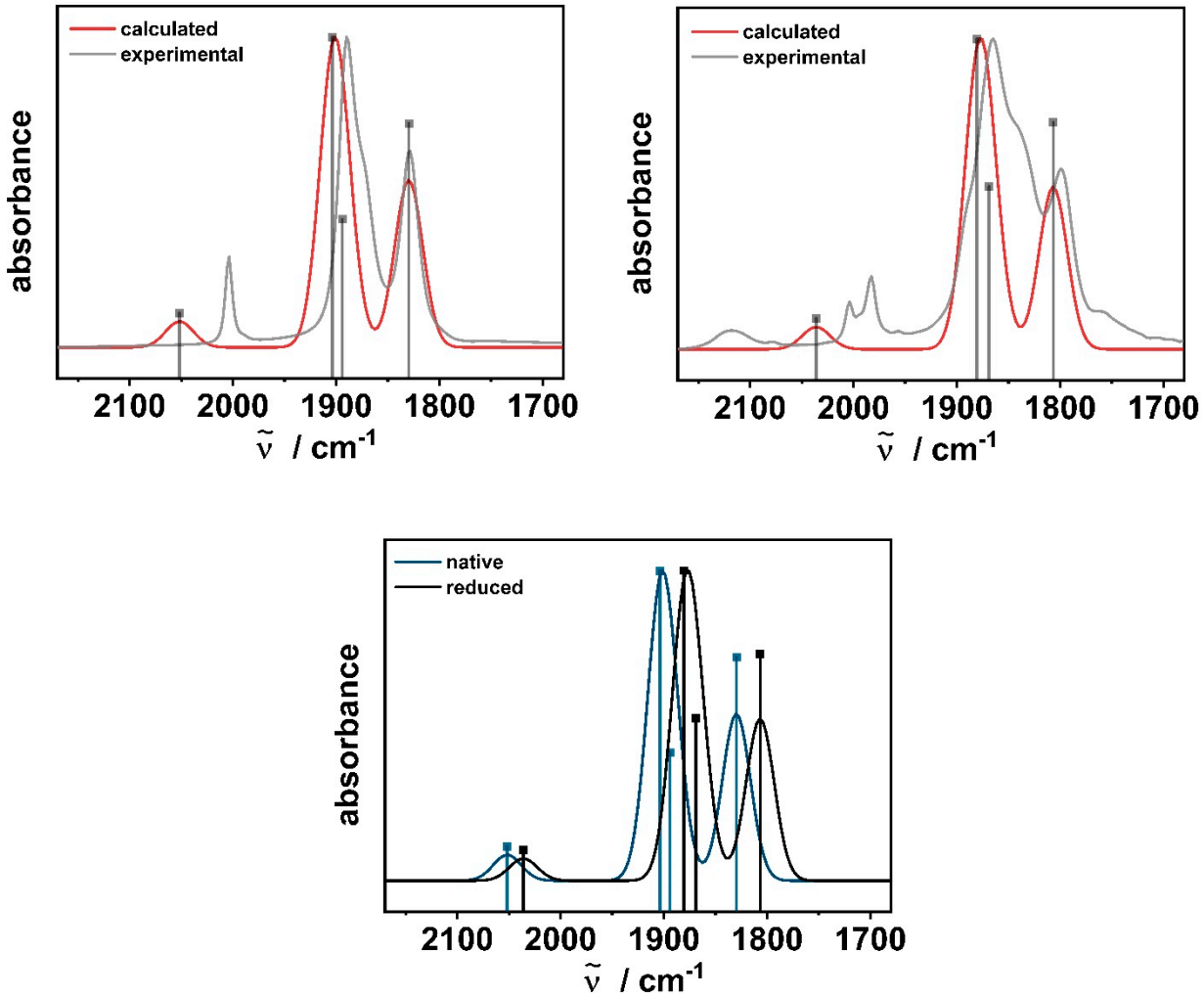

Figure S15. Top left: Calculated (red) and experimental (grey) IR spectra of [Mo(**C–C**)(CO)$_4$], Top right: Calculated (red) and experimental (grey) IR spectra of [Mo(**C–C**)(CO)$_4$]$^-$ and bottom centered: Overlay of calculated [Mo(**C–C**)(CO)$_4$] (blue) and [Mo(**C–C**)(CO)$_4$]$^-$ (black) (B3LYP/RIJCOSX/D3BJ/def2-TZVP, FWHM = 32).

S4.30 IR-Spectroelectrochemistry of [W(C–C)(CO)$_4$]

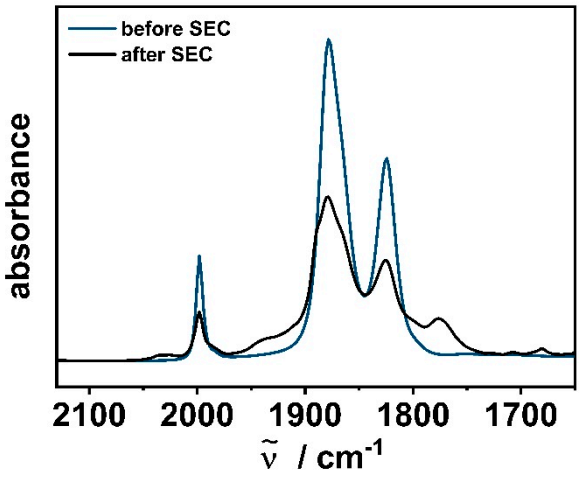

Figure S16. Changes in the IR spectra of [W(**C–C**)(CO)$_4$] in CH$_3$CN/0.1 M Bu$_4$NPF$_6$ with a Au working electrode after the first reduction.

Table S5. Experimental and calculated changes (B3LYP/RIJCOSX/D3BJ/def2-TZVP) in the CO frequencies of [W(**C–C**)(CO)$_4$] in CH$_3$CN/0.1 M Bu$_4$NPF$_6$ with a Au working electrode during the first reduction.

		$\tilde{\upsilon}$ (CO) / cm^{-1}								
exp.	**[W(C–C)(CO)$_4$]**	1998	1878	1871	1824					
	[W(C–C)(CO)$_4$]$^-$	2119[a]	2065	1986	1877	1853	1795	1783	1754	1730
calc.	**[W(C–C)(CO)$_4$]**	2047	1893	1889	1822					
	[W(C–C)(CO)$_4$]$^-$	2027	1864	1856	1790					

[a] free CO

S4.31 Calculated IR Spectra of $[W(C–C)(CO)_4]$ and $[W(C–C)(CO)_4]^-$

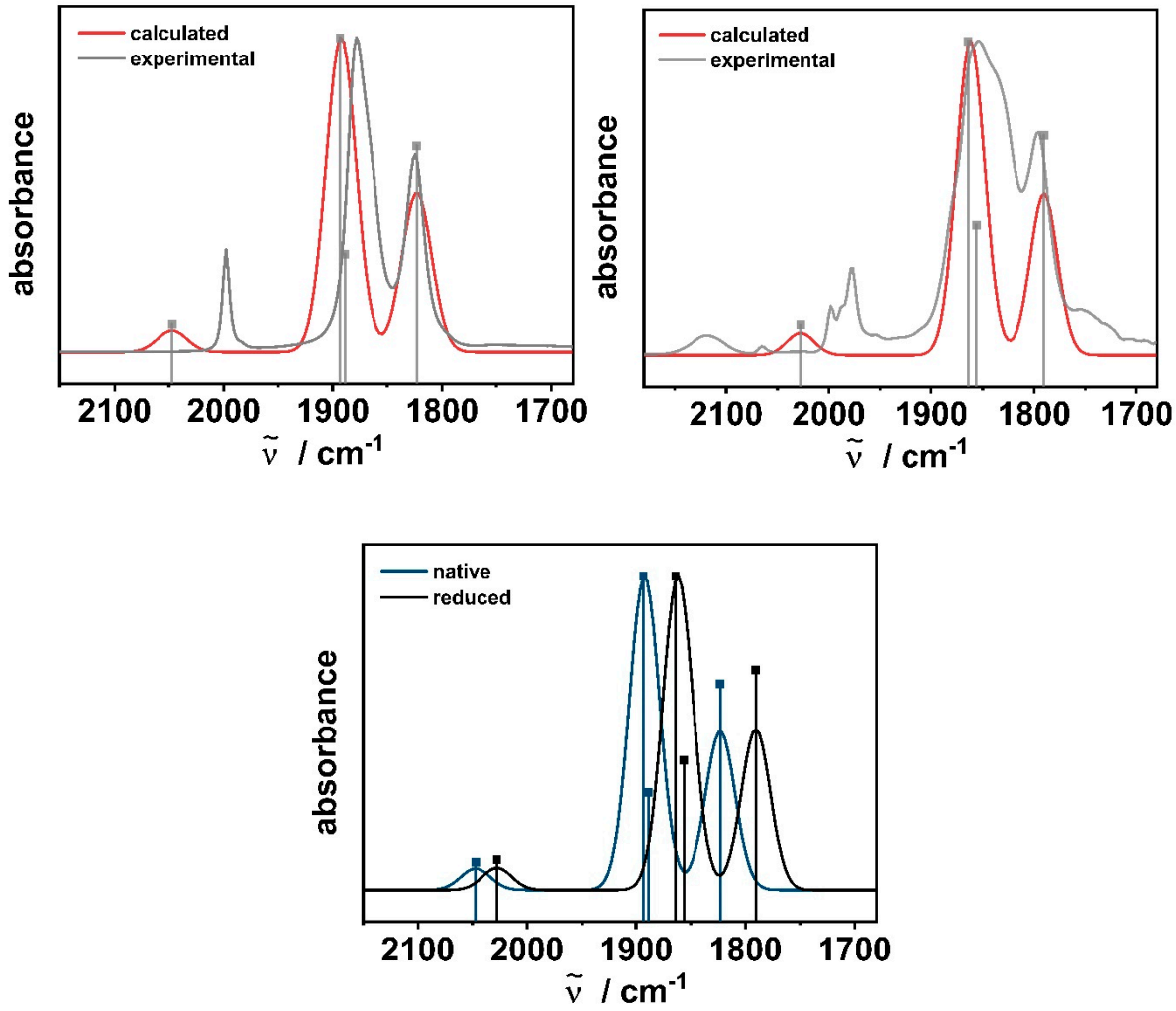

Figure S17. Top left: Calculated (red) and experimental (grey) IR spectra of $[W(\mathbf{C–C})(CO)_4]$, Top right: Calculated (red) and experimental (grey) IR spectra of $[W(\mathbf{C–C})(CO)_4]^-$ and bottom centered: Overlay of calculated $[W(\mathbf{C–C})]$ (blue) and $[W(\mathbf{C–C})(CO)_4]^-$ (black) (B3LYP/RIJCOSX/D3BJ/ZORA/def2-TZVP, FWHM = 32).

S4.40 IR-Spectroelectrochemistry of [W(C–N)(CO)$_4$]

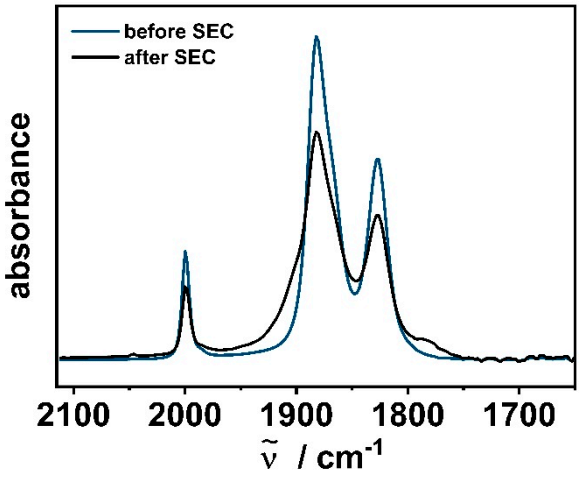

Figure S13. Changes in the IR spectra of [W(**C–N**)(CO)$_4$] in CH$_3$CN/0.1 M Bu$_4$NPF$_6$ with a Au working electrode after the first reduction.

Table S6. Experimental and calculated changes (B3LYP/RIJCOSX/D3BJ/def2-TZVP) in the CO frequencies of [W(**C–N**)(CO)$_4$] in CH$_3$CN/0.1 M Bu$_4$NPF$_6$ with a Au working electrode during the first reduction.

		$\tilde{\upsilon}$ **(CO) / cm^{-1}**			
exp.	**[W(C–N)(CO)$_4$]**	2000	1882	1873 (sh)	1826
	[W(C–N)(CO)$_4$]$^-$	1979	1878	1838	1792
calc.	**[W(C–N)(CO)$_4$]**	2039	1892	1881	1830
	[W(C–N)(CO)$_4$]$^-$	2018	1853	1843	1790

S4.41 Calculated IR Spectra of [W(C–N)(CO)$_4$] and [W(C–N)(CO)$_4$]$^-$

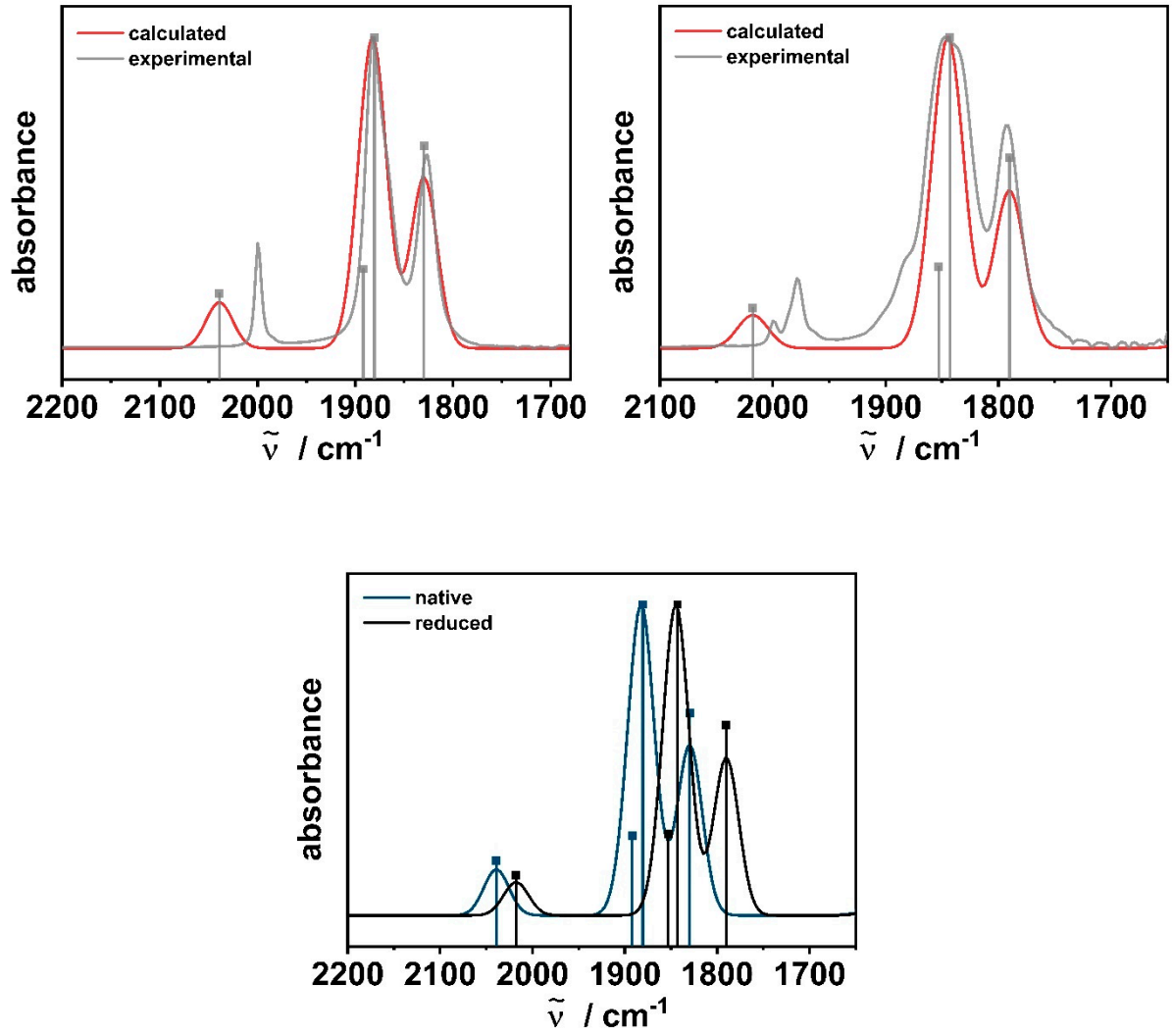

Figure S19. Top left: Calculated (red) and experimental (grey) IR spectra of [W(**C–N**)(CO)$_4$], Top right: Calculated (red) and experimental (grey) IR spectra of [W(**C–N**)(CO)$_4$]$^-$ and bottom centered: Overlay of calculated [W(**C–N**)(CO)$_4$] (blue) and [W(**C–N**)(CO)$_4$]$^-$ (black) (B3LYP/RIJCOSX/D3BJ/ZORA/def2-TZVP, FWHM = 32).

S5. UV/vis/NIR-Spectroelectrochemistry

S5.10 UV/vis/NIR-Spectroelectrochemistry of [Cr(C–C)(CO)$_4$]

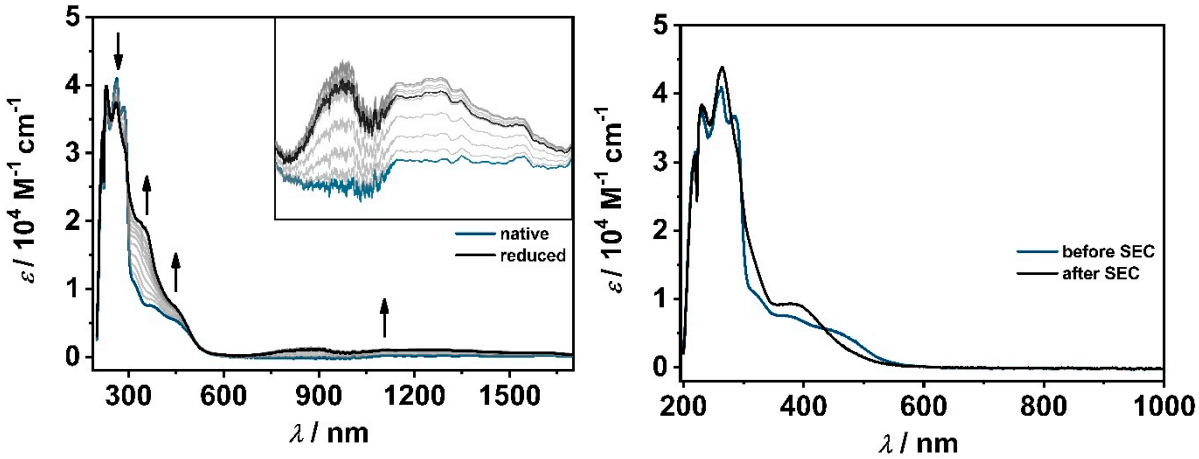

Figure S20. Changes in the UV/VIS spectra of [Cr(**C–C**)(CO)$_4$] (left, Inset: 600–1800 nm) in CH_3CN/0.1 M Bu_4NPF_6 during the first reduction with a Au working electrode and after UV/vis/NIR-SEC (right).

S5.20 UV/vis/NIR-Spectroelectrochemistry of [Mo(C–C)]

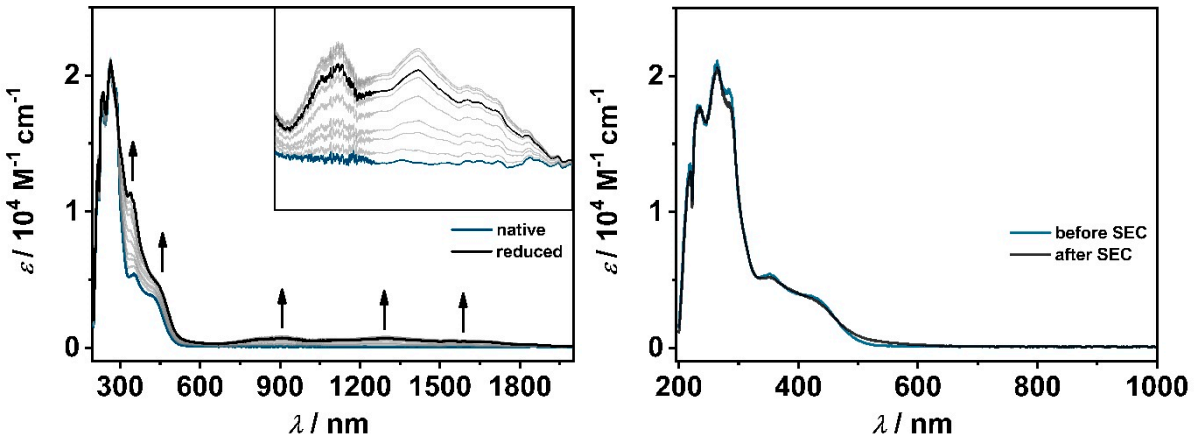

Figure S21. Changes in the UV/VIS spectra of [Mo(**C–C**)(CO)$_4$] (left, Inset: 600–2000 nm) in CH_3CN/0.1 M Bu_4NPF_6 during the first reduction with a Au working electrode and after UV/vis/NIR-SEC (right).

S5.30 UV/vis/NIR-Spectroelectrochemistry of [W(C–C)(CO)$_4$]

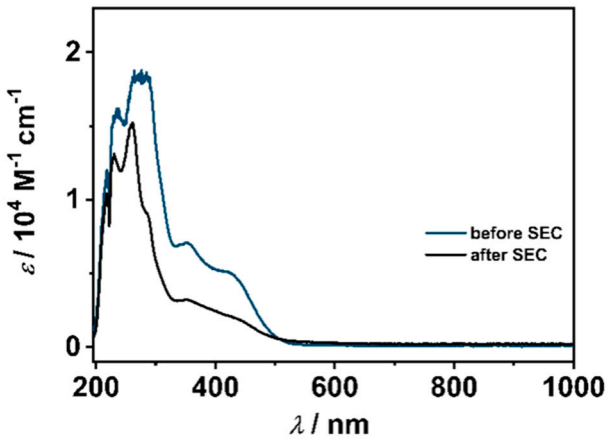

Figure S22. Changes in the UV/VIS spectra of [W(**C–C**)(CO)$_4$ in CH_3CN/0.1 M Bu_4NPF_6 after the first reduction with a Au working electrode.

S5.40 UV/vis/NIR-Spectroelectrochemistry of [W(C–N)(CO)$_4$]

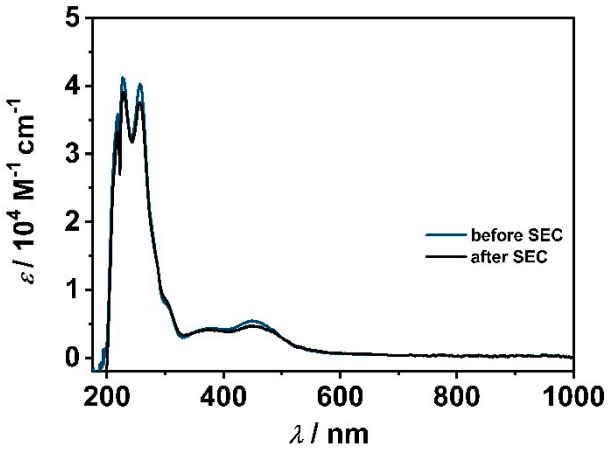

Figure S23. Changes in the UV/VIS spectra of [W(**C–N**)(CO)$_4$] in CH_3CN/0.1 M Bu_4NPF_6 after the first reduction with a Au working electrode.

S6. TD-DFT Calculations

S6.10 TD-DFT Calculations of $[Cr(C–C)(CO)_4]^-$

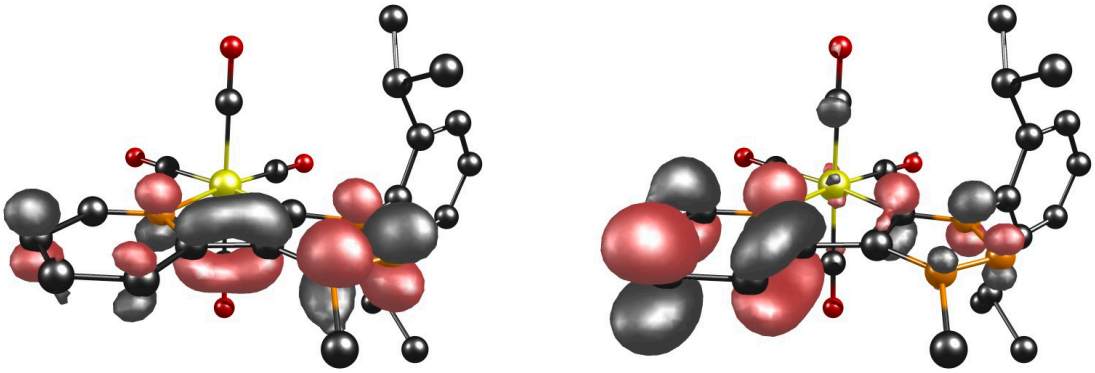

Figure S24. α-HOMO (left) and α-LUMO (right) of complex $[Cr(\mathbf{C–C})(CO)_4]^-$.

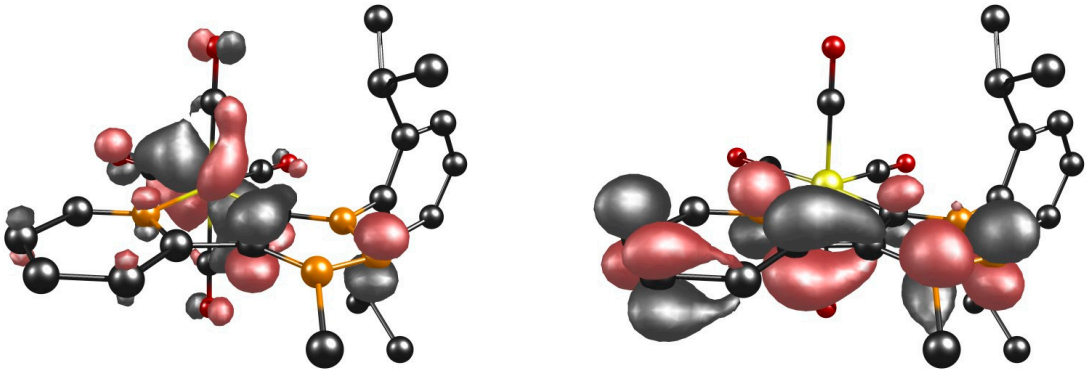

Figure S25. β-HOMO (left) and β-LUMO (right) of complex $[Cr(\mathbf{C–C})(CO)_4]^-$.

Table S7. Energies of selected orbitals.

MO	Energy / eV
$[\mathbf{Cr(C-C)(CO)_4}]^-_{\alpha-\mathbf{HOMO}}$	−2.9139
$[\mathbf{Cr(C-C)(CO)_4}]^-_{\alpha-\mathbf{LUMO}}$	−0.7303
$[\mathbf{Cr(C-C)(CO)_4}]^-_{\beta-\mathbf{HOMO}}$	−4.7504
$[\mathbf{Cr(C-C)(CO)_4}]^-_{\beta-\mathbf{LUMO}}$	−1.0098

Table S8. Selected experimental UV/vis data of $[Cr(\mathbf{C–C})(CO)_4]^-$ together with selected TD-DFT calculations.

State	$\lambda_{exp}(\lambda_{DFT})$ / nm	ε / 10^4 M^{-1} cm^{-1}(f)	Main contributing excitation (%)
1	1233 (1042)	0.09 (0.021)	α-HOMO → α-LUMO (92)
2	1233 (908)	0.09 (0.004)	α-HOMO → α-LUMO+1 (99)
5	874 (767)	0.10 (0.008)	α-HOMO → α-LUMO+3 (21)
			α-HOMO → α-LUMO+4 (77)
3	874 (712)	0.10 (0.028)	α-HOMO → α-LUMO+2 (71)
			α-HOMO → α-LUMO+3 (17)
4	874 (690)	0.10 (0.013)	α-HOMO → α-LUMO+2 (27)
			α-HOMO → α-LUMO+3 (55)
			α-HOMO → α-LUMO+4 (13)
6	874 (661)	0.10 (0.005)	α-HOMO → α-LUMO+5 (95)
12	444 (420)	0.74 (0.052)	α-HOMO → α-LUMO+6 (20)
			β-HOMO–1 → β-LUMO (23)
			β-HOMO → β-LUMO (39)
19	347 (386)	1.90 (0.014)	α-HOMO–2 → α-LUMO (55)
			α-HOMO → α-LUMO+8 (12)
23	289 (362)	3.07 (0.040)	α-HOMO–3 → α-LUMO (31)
			α-HOMO → α-LUMO+10 (10)
			β-HOMO–2 → β-LUMO (95)

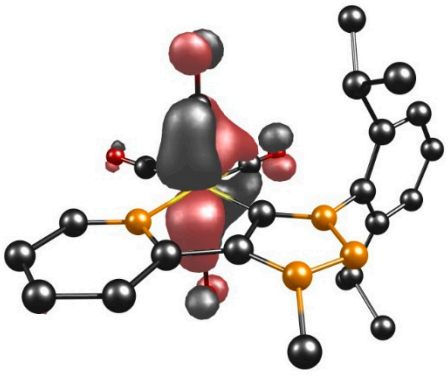

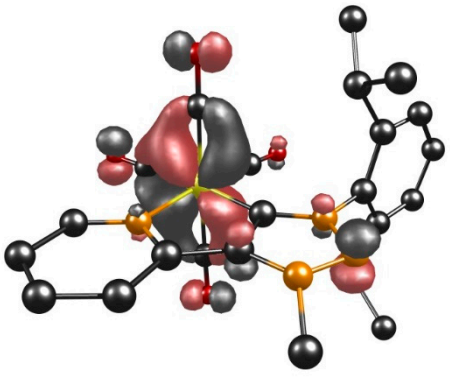

α-HOMO–3

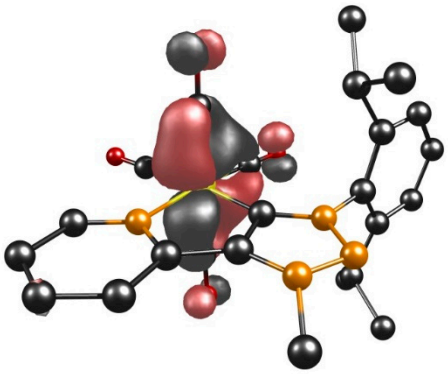

α-HOMO–2

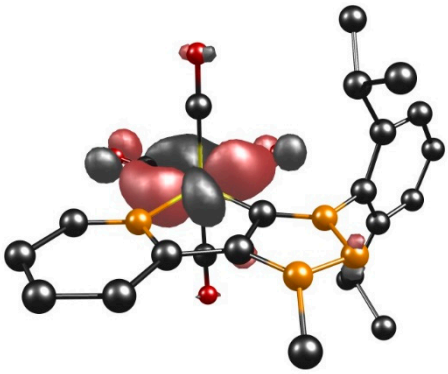

β-HOMO–2

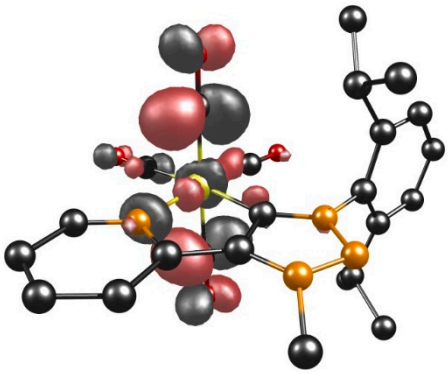

β-HOMO–1

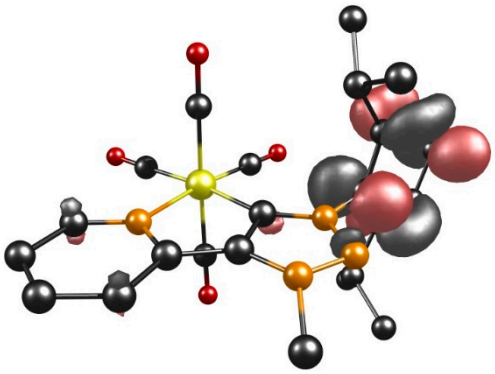

α-LUMO+1

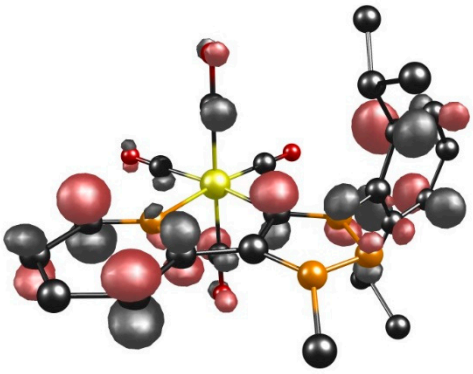

α-LUMO+2

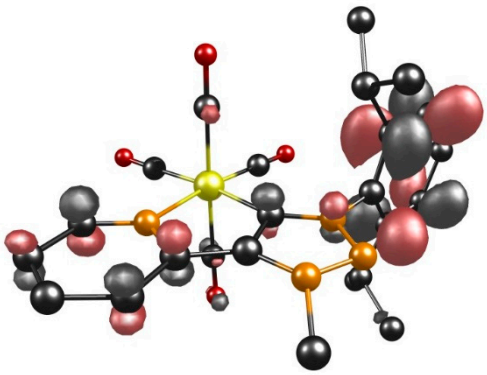

α-LUMO+3

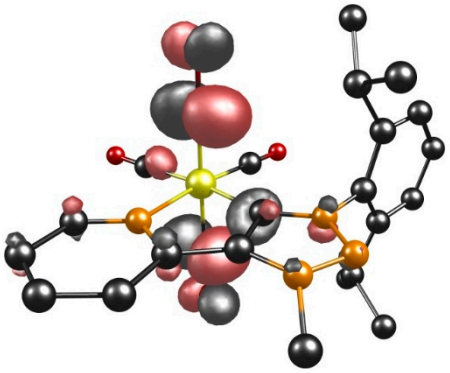

α-LUMO+4

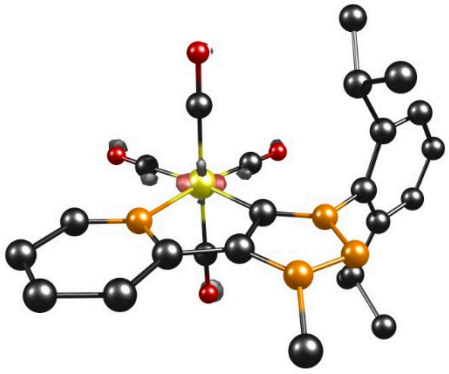

α-LUMO+5

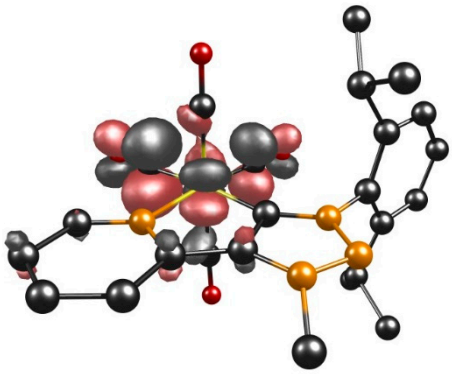

α-LUMO+6

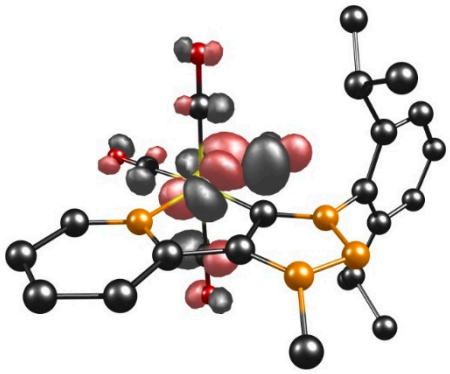

α-LUMO+8

α-LUMO+10

Figure S26. Involved TD-DFT orbitals of complex [Cr(**C–C**)$(CO)_4]^-$.

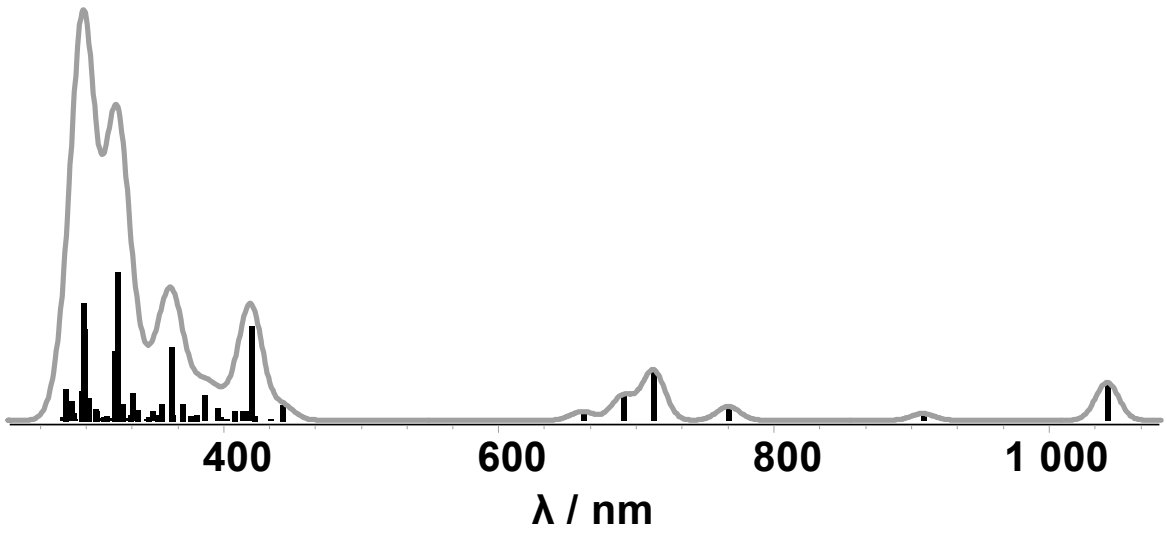

Figure S27. Calculated TD-DFT spectrum with discrete transitions of $[Cr(C–C)(CO)_4]^-$.

Table S9. Selected MO energies of $[Cr(\mathbf{C–C})(CO)_4]^-$.

[Cr(C–C)(CO)$_4$]	
MO	**Energy / eV**
***α*-HOMO–3**	−5.0233
***α*-HOMO–2**	−4.9339
***β*-HOMO–2**	−5.0087
***β*-HOMO–1**	−4.7884
***α*-LUMO+1**	−0.4520
***α*-LUMO+2**	−0.2976
***α*-LUMO+3**	−0.1509
***α*-LUMO+4**	−0.1018
***α*-LUMO+5**	0.0296
***α*-LUMO+6**	0.7195
***α*-LUMO+8**	0.9970
***α*-LUMO+10**	1.3273

Table S10. XYZ coordinates of optimized $[Cr(\mathbf{C–C})(CO)_4]^-$.

	x	y	z
Cr	1.003091865399	10.144308109284	4.920620955770
N	-0.327529613304	11.225048571129	3.556597075598
C	2.304260792897	11.157578850925	3.660889243339
C	2.300027319261	9.396995879807	5.968236897578
C	-0.364731194992	9.394525104065	5.895184777627
C	1.036980981727	8.588233261823	3.857503224277
C	1.022708211846	11.703966211450	5.989811553496
C	0.295958421057	12.073713175478	2.652694018438
C	-1.659205523688	11.179635670584	3.580707084696
C	1.703000946840	12.027859460950	2.747089960653
N	3.620330589328	11.346991047963	3.481090056778
O	3.123885089854	8.918171908384	6.638880517296
O	-1.212475404048	8.889015251422	6.518466812216
O	1.066078887157	7.592487662849	3.271722327061
O	1.050292661236	12.659830542034	6.635347014676
C	-0.490466987621	12.854463965926	1.768009516708
C	-2.478828931017	11.927592514150	2.749422737846

H	-2.093967690411	10.505914848922	4.307849677130
N	2.724170654548	12.669470884089	2.032572408242
N	3.954690278002	12.286059105824	2.525111858559
C	4.707546870760	10.657915295331	4.108296786689
H	-0.009393636320	13.508594022799	1.056758953974
C	-1.862569036132	12.781823124953	1.818984565904
H	-3.553282620709	11.841686424139	2.827347214182
C	2.667145160162	14.009141791203	1.480040107077
C	5.126706771478	9.439322300204	3.557527579024
C	5.310442692325	11.221073247086	5.240728960465
H	-2.460990166273	13.382418909927	1.145117848779
H	3.633630841160	14.236057282542	1.035288658247
H	2.447745900655	14.748756438091	2.259162216749
H	1.906200551001	14.069370185083	0.706030217281
C	6.256619703008	8.835848146394	4.108490210903
C	4.335745899669	8.768455060597	2.448855757613
C	4.710228895259	12.436002825361	5.927808482522
C	6.437379277906	10.580944381017	5.756019126606
H	6.613771265882	7.898076612775	3.704977147245
C	6.921021899080	9.414074760809	5.181307457013
H	3.296769147441	9.056634710685	2.600443842596
C	4.742399702485	9.250507472730	1.048308264630
C	4.397384375359	7.241944490694	2.523087684508
H	3.636211725899	12.386644482679	5.749124553782
C	5.213370240599	13.762549407850	5.342981379669
C	4.923123382583	12.420948340955	7.443912235763
H	6.932463045209	10.986651054147	6.627426521221
H	7.798111999138	8.931635479419	5.595696167752
H	4.140486996235	8.742109223441	0.291554334159
H	5.793576962160	9.022564125236	0.851400090421
H	4.589006412587	10.324974654000	0.944829020697
H	3.667755185932	6.814650707018	1.833535552300
H	4.166585182340	6.879723256398	3.526079132096
H	5.380544248422	6.860917449993	2.237783551776
H	4.986462945283	13.828981270830	4.278929496535
H	6.293691966507	13.857493536625	5.484932206895
H	4.731532285160	14.599516481732	5.853806569160
H	4.629356460343	11.464666923525	7.879966768611
H	4.319770125660	13.204817569911	7.904645122493
H	5.965277987676	12.613826526761	7.708989496680

S6.20 TD-DFT Calculations of $[Mo(C–C)(CO)_4]$ and $[Mo(C–C)(CO)_4]^–$

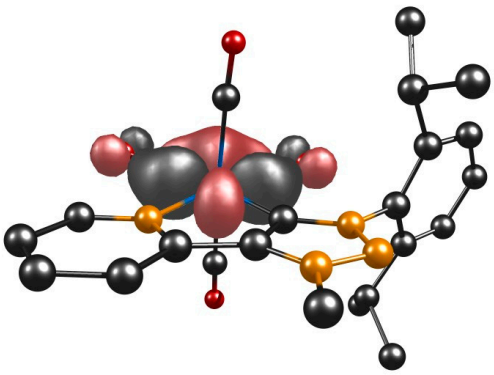

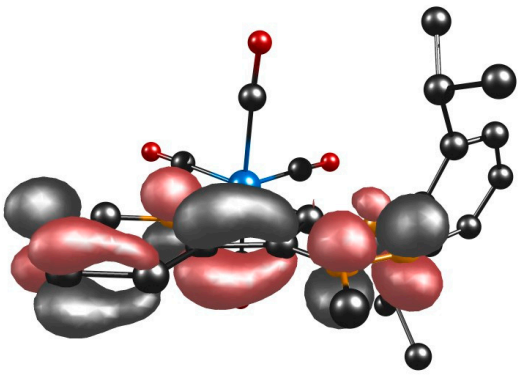

Figure S28. HOMO (left) and LUMO (right) of complex [Mo(**C–C**)$(CO)_4$].

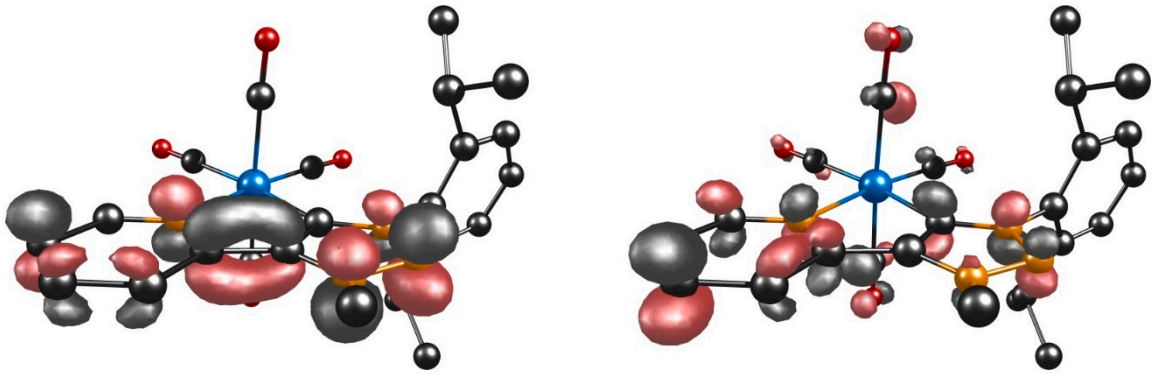

Figure S29. α-HOMO (left) and α-LUMO (right) of complex [Mo(**C–C**)$(CO)_4]^-$.

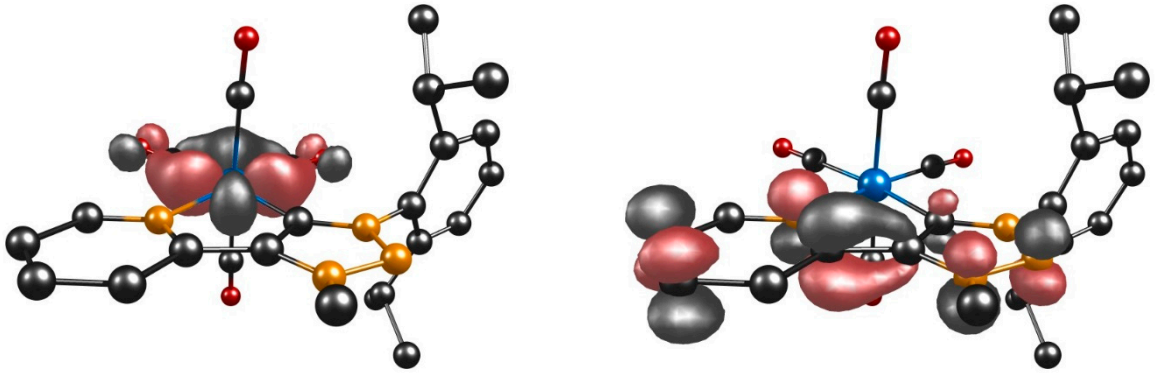

Figure S30. β-HOMO (left) and β-LUMO (right) of complex [Mo(**C–C**)$(CO)_4]^-$.

Table S11. Energies and compositions of selected orbitals.

MO	Energy / eV
$[\mathbf{Mo(C-C)(CO)_4}]_{\mathbf{HOMO}}$	−5.1001
$[\mathbf{Mo(C-C)(CO)_4}]_{\mathbf{LUMO}}$	−2.0257
$[\mathbf{Mo(C-C)(CO)_4}]^-_{\boldsymbol{\alpha}\mathbf{-HOMO}}$	−2.3462
$[\mathbf{Mo(C-C)(CO)_4}]^-_{\boldsymbol{\alpha}\mathbf{-LUMO}}$	−0.7250
$[\mathbf{Mo(C-C)(CO)_4}]^-_{\boldsymbol{\beta}\mathbf{-HOMO}}$	−4.6769
$[\mathbf{Mo(C-C)(CO)_4}]^-_{\boldsymbol{\beta}\mathbf{-LUMO}}$	−0.6866

Table S12. Selected experimental UV/vis data of [Mo(C–C)] together with selected TD-DFT calculations.

State	$\lambda_{exp}(\lambda_{DFT})$ / nm	ε / 10^4 M^{-1} cm^{-1}(f)	Main contributing excitation (%)
3	422 (507)	0.38 (0.048)	HOMO–2 → LUMO (78) HOMO–1 → LUMO (18)
4	354 (373)	0.54 (0.032)	HOMO → LUMO+1 (33) HOMO → LUMO+2 (58)
10	305 (330)	0.94 (0.070)	HOMO–2 → LUMO+1 (45) HOMO–2 → LUMO+4 (16) HOMO–1 → LUMO+1 (15)

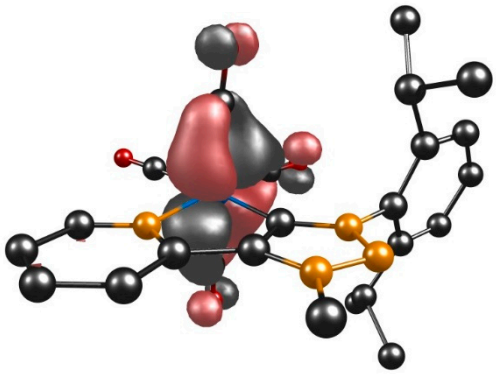

HOMO–2

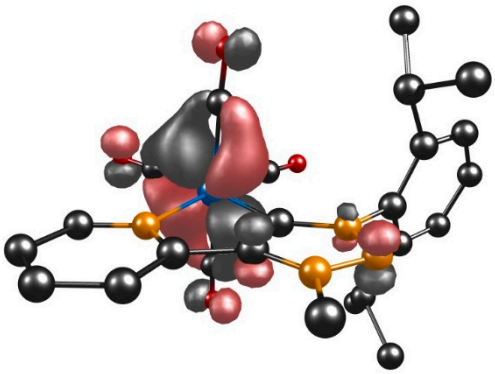

HOMO–1

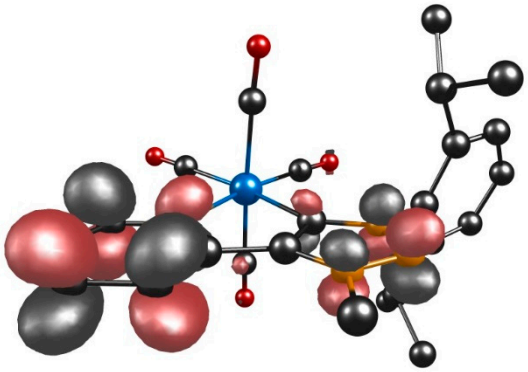

LUMO+1

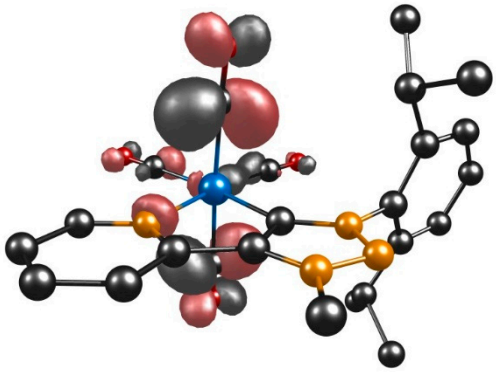

LUMO+2

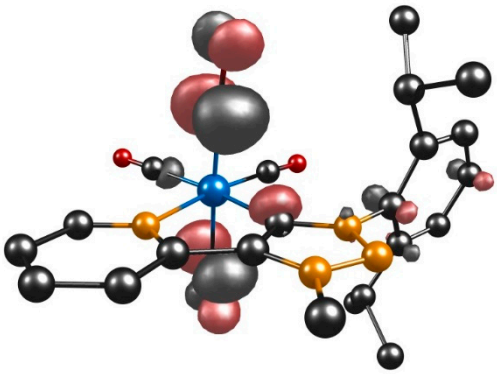

LUMO+4

Figure S31. Involved TD-DFT orbitals of complex [Mo(**C–C**)(CO)$_4$].

Table S13. Selected experimental UV/vis data of [Mo(**C–C**)(CO)$_4$]$^-$ together with selected TD-DFT calculations.

State	$\lambda_{exp}(\lambda_{DFT})$ / nm	ε / M^{-1} cm^{-1}(f)	Main contributing excitation (%)
2	1300 (1262)	0.07 (0.003)	α-HOMO → α-LUMO+1 (86)
1	1300 (1096)	0.07 (0.029)	α-HOMO → α-LUMO+1 (93)
3	911 (950)	0.07 (0.002)	α-HOMO → α-LUMO+2 (86)
5	911 (852)	0.07 (0.006)	α-HOMO → α-LUMO+3 (22)
			α-HOMO → α-LUMO+5 (71)
4	911 (761)	0.07 (0.032)	α-HOMO → α-LUMO+2 (13)
			α-HOMO → α-LUMO+3 (22)
10	435 (457)	0.49 (0.008)	α-HOMO → α-LUMO+7 (70)

15	435 (408)	0.49 (0.016)	α-HOMO–2 → α-LUMO+2 (14) β-HOMO–1 → β-LUMO (22) β-HOMO–1 → β-LUMO+2 (29)
18	340 (402)	1.14 (0.037)	β-HOMO–2 → β-LUMO (14) β-HOMO–1 → β-LUMO (39)
30	340 (367)	1.14 (0.053)	α-HOMO–3 → α-LUMO (22) α-HOMO–3 → α-LUMO+1 (22) α-HOMO–3 → α-LUMO+3 (22) α-HOMO–3 → α-LUMO+3 (22)

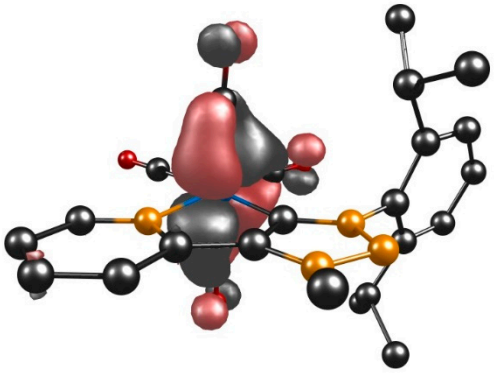

α-HOMO–3

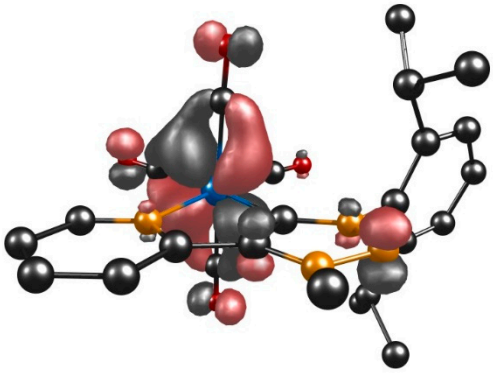

α-HOMO–2

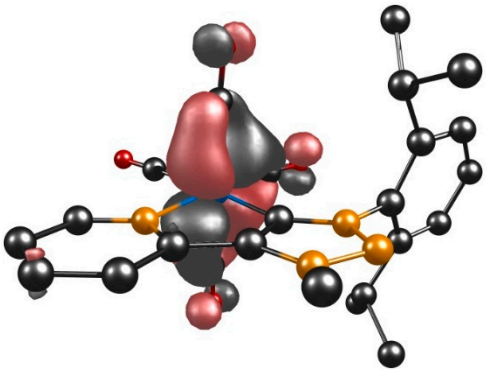

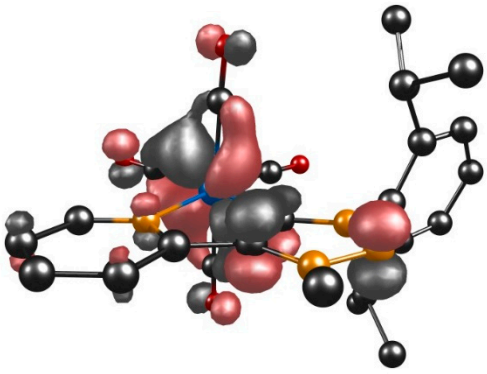

β-HOMO–2

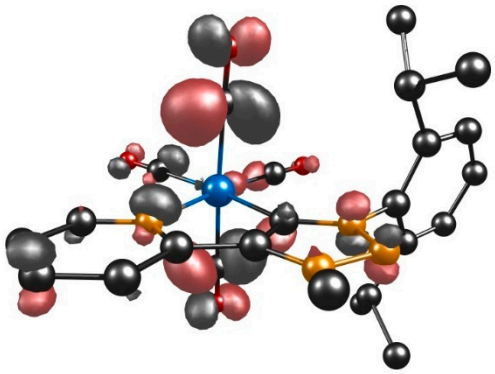

β-HOMO–1

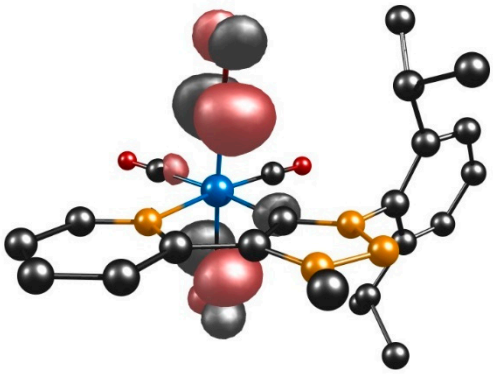

α-LUMO+1

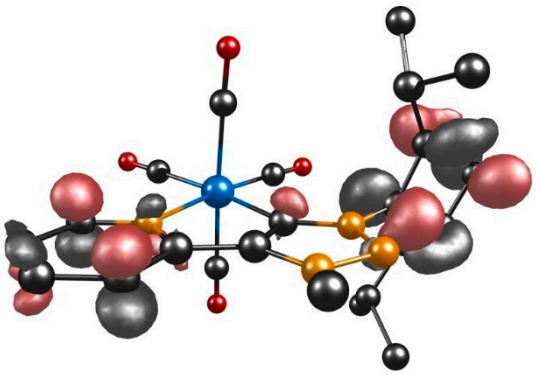

α-LUMO+2

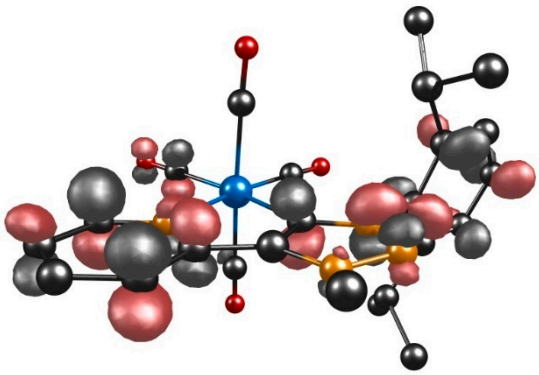

α-LUMO+3

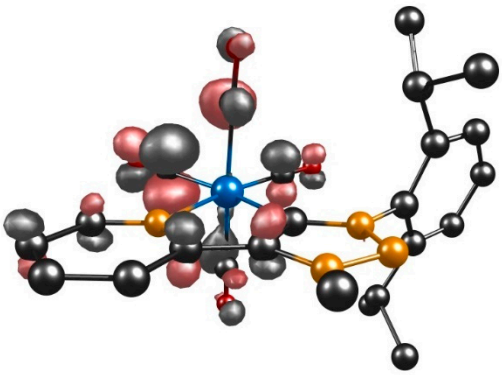

α-LUMO+5

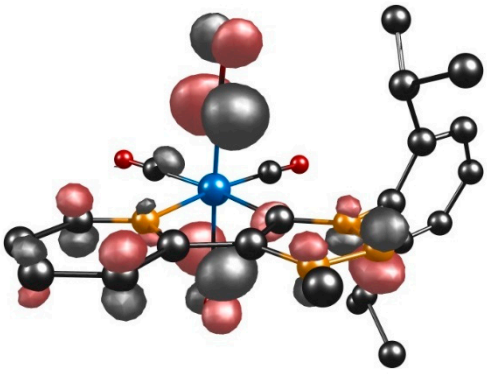

***α*-LUMO+7** ***β*-LUMO+2**

Figure S32. Involved TD-DFT orbitals of complex [Mo(**C–C**)$(CO)_4$]$^-$.

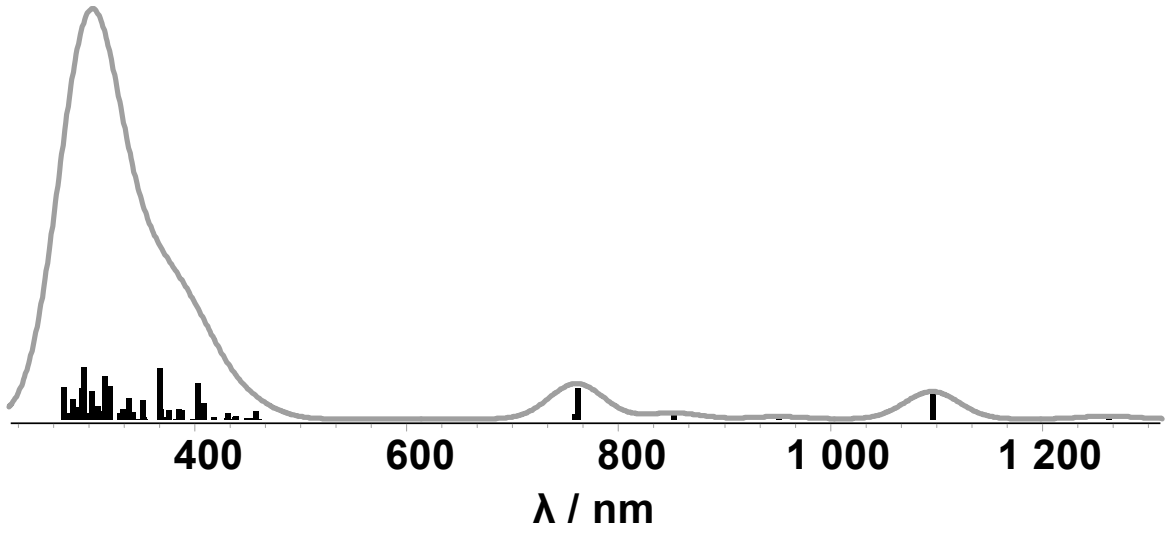

Figure S33. Calculated TD-DFT spectrum with discrete transitions of [Mo(**C–C**)$(CO)_4$]$^-$.

Table S14. Selected MO energies of [Mo(**C–C**)$(CO)_4$] and [Mo(**C–C**)$(CO)_4$]$^-$.

[Mo(C–C)$(CO)_4$]		**[Mo(C–C)$(CO)_4$]$^-$**	
MO	**Energy / eV**	**MO**	**Energy / eV**
HOMO–2	−5.3710	***α*-HOMO–3**	−4.8700
HOMO–1	−5.3161	***α*-HOMO–2**	−4.6771
LUMO+1	−1.3513	***β*-HOMO–2**	−4.9296
LUMO+2	−1.0433	***β*-HOMO–1**	−4.7613

LUMO+4	−0.6818	***α*-LUMO+1**	−0.6687
		***α*-LUMO+2**	−0.3627
		***α*-LUMO+3**	−0.2927
		***α*-LUMO+5**	−0.0365
		***α*-LUMO+7**	0.7661
		***β*-LUMO+2**	−0.3680

Table S15. XYZ coordinates of optimized [Mo(**C–C**)$(CO)_4$].

	x	y	z
Mo	5.668613958431	4.650569521145	10.617888820018
N	6.901830430287	3.130103905852	11.894751730907
C	4.245216226792	3.466603015282	11.807589734835
C	7.227292556468	5.470029527646	9.673809841092
C	4.381286167989	5.818767111593	9.716868051357
C	5.828432400970	6.139498068707	12.004413652109
C	5.413751519780	3.265370575462	9.131765563486
C	6.219714151011	2.265020065428	12.695622508639
C	8.235960732089	3.049566363961	11.863826684594
C	4.787517757654	2.474066358776	12.623496700356
N	2.911233189420	3.297462786678	11.997712402623
O	8.139597428533	5.952035275930	9.138008765925
O	3.587006686751	6.512365556998	9.223304263589

O	5.901873824219	7.052489454306	12.703000621655
O	5.222095058848	2.502489557293	8.292947186463
C	6.879235880261	1.310552100515	13.466044402173
C	8.956811362364	2.125882816812	12.605488517058
H	8.739915444187	3.752598838666	11.216529509699
N	3.749136227340	1.822178613032	13.218719753779
N	2.593466720460	2.317433153420	12.850945122019
C	1.827128317848	3.988281218921	11.349373890874
H	6.325670416683	0.631466478262	14.093750060572
C	8.263559644013	1.240678591348	13.419761107281
H	10.034907741996	2.104733301435	12.534614531645
C	3.756060140114	0.688541559132	14.135257786899
C	1.454642918027	5.246869461835	11.830545528929
C	1.206781751130	3.355050340446	10.267614171866
H	8.789107400494	0.504171881657	14.012260146749
H	2.724544222174	0.457664197806	14.380353398778
H	4.302799959251	0.957573571930	15.036179674690
H	4.224938956038	-0.162233063672	13.645382335067
C	0.340855560938	5.842007298500	11.241081735879
C	2.258533092474	5.942953573559	12.913063768631
C	0.096146926376	3.992642871542	9.713541258751
C	1.749967307816	2.062445155923	9.683767924848
H	0.007066250449	6.810944020296	11.585067402743
C	-0.343865673493	5.210821131244	10.210421728503
H	3.297256261827	5.649129611574	12.762184364496
C	1.851876097642	5.496037119326	14.325586309310
C	2.206553099173	7.466502975142	12.799199064672
H	-0.421176056340	3.538594990354	8.879775253163
C	1.681381818492	2.049234170690	8.155052388361
H	2.805298785138	2.004285256538	9.954938518679
C	1.058275141373	0.818656745098	10.258331397842
H	-1.209424347438	5.689707947957	9.769532363938
H	0.799563910067	5.723387454444	14.513682942111
H	2.450567369181	6.026401614254	15.068621093844
H	2.006978211570	4.425969978628	14.470888909791
H	2.445486834578	7.798429851497	11.787791768808
H	2.934815099314	7.905765030943	13.482450415577
H	1.224348598099	7.859836862432	13.069388721006
H	2.212898875312	1.176578899348	7.773005913636
H	2.141077738229	2.941940114590	7.728768233950
H	0.651276937612	1.990143946531	7.798651720501
H	-0.010572590795	0.832925903267	10.030199244263
H	1.183634553852	0.760246176843	11.339376749811
H	1.488241006930	-0.080978907123	9.812864341160

Table S16. XYZ coordinates of optimized $[Mo(\mathbf{C–C})(CO)_4]^-$.

	x	**y**	**z**
Mo	5.645743103638	4.641522907645	10.642365229029
N	6.898350211141	3.157502644334	11.893496614530
C	4.224696385226	3.459659255204	11.862661263279
C	7.186916065898	5.460048528618	9.684676430772
C	4.344801571738	5.795993150927	9.740303529494
C	5.813696810313	6.139595353416	12.010820049962
C	5.391506043808	3.241147929012	9.173979589424
C	6.193553498842	2.279666254158	12.719965328765
C	8.231344625259	3.069793148280	11.860551265593
C	4.794661953848	2.466584842233	12.677491507957
N	2.904770818675	3.311882980912	12.048057736577
O	8.093786430535	5.950131487818	9.136611006650
O	3.550941711075	6.488641773892	9.237100661146

O	5.898267690258	7.064981002884	12.697107284937
O	5.214021352481	2.472078769728	8.334418952232
C	6.906442371117	1.329391799294	13.497085238908
C	8.974439331869	2.163617185455	12.595770970785
H	8.727428511021	3.771192724227	11.201489302997
N	3.743649776120	1.822970630071	13.328298518205
N	2.536321521298	2.318938657151	12.916402037719
C	1.838338378213	3.996974761598	11.380832504443
H	6.366263072889	0.649505694931	14.138352852003
C	8.275925277090	1.270828811048	13.437455095534
H	10.051470541797	2.146664342973	12.510498024792
C	3.734190134000	0.537760727635	13.990342716485
C	1.457852567261	5.267574956151	11.829023830105
C	1.209599420310	3.350342918052	10.309382348368
H	8.812734694650	0.543267559518	14.033324775268
H	2.722959599660	0.348781200766	14.342698932363
H	4.408126243340	0.539462121577	14.844880303580
H	4.028749219247	-0.259115626236	13.299770852917
C	0.342520908363	5.851701037333	11.230137059880
C	2.264207015177	5.992686737940	12.890573611405
C	0.095214421792	3.972595988979	9.744782550663
C	1.760666573948	2.057210923681	9.735156702296
H	0.010589987398	6.828512251141	11.554518958623
C	-0.348143581922	5.199744048779	10.216659606676
H	3.300367695573	5.691703779895	12.742167432893
C	1.864728601058	5.576728408315	14.314066506562
C	2.212721383580	7.513220199654	12.739704962032
H	-0.422211954030	3.500011293397	8.920643879256
C	1.741640808957	2.061564815888	8.204676732962
H	2.804351457275	1.992960797565	10.044180378977
C	1.046468014985	0.812697596438	10.277583100169
H	-1.216525158274	5.668176084707	9.769211723284
H	0.815494167059	5.816899429472	14.506999829048
H	2.472892488816	6.114877279351	15.044496080175
H	2.013475503411	4.507066338925	14.468401854047
H	2.448351436444	7.818952584208	11.719059500059
H	2.944389673951	7.969914328773	13.408199109642
H	1.232059856016	7.916072261703	13.003227557422
H	2.271503529483	1.185445026279	7.827297323601
H	2.229386326332	2.951885030955	7.805358252320
H	0.722845858729	2.025445964490	7.813593425514
H	-0.017588577319	0.834394471918	10.025795361002
H	1.156532316674	0.751332735167	11.359990197246
H	1.479702313909	-0.086697908223	9.833363549428

S6.30 TD-DFT Calculations of $[W(C–C)(CO)_4]$ and $[W(C–C)(CO)_4]^-$

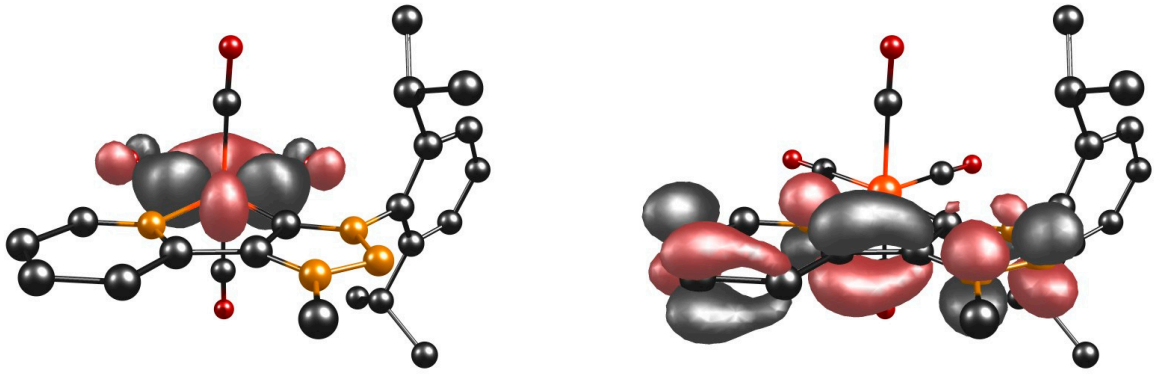

Figure S34. HOMO (left) and LUMO (right) of complex [W(**C–C**)$(CO)_4$].

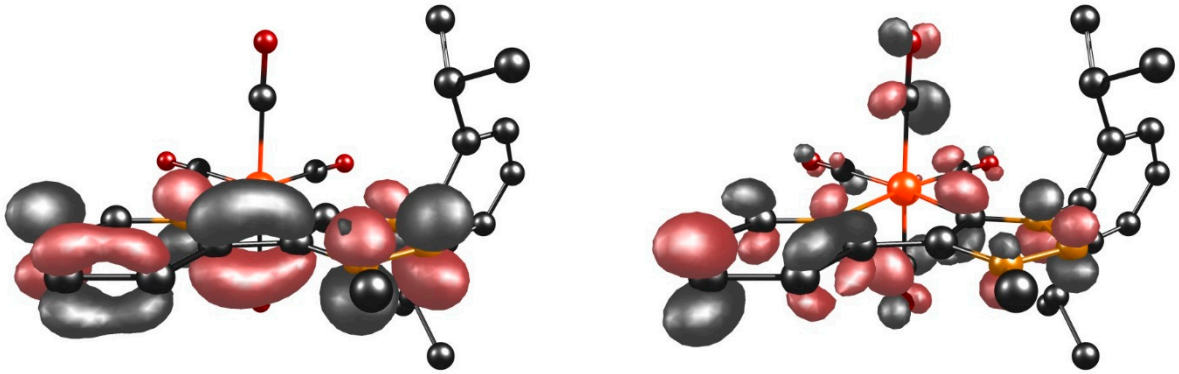

Figure S35. α-HOMO (left) and α-LUMO (right) of complex [W(**C–C**)$(CO)_4]^-$.

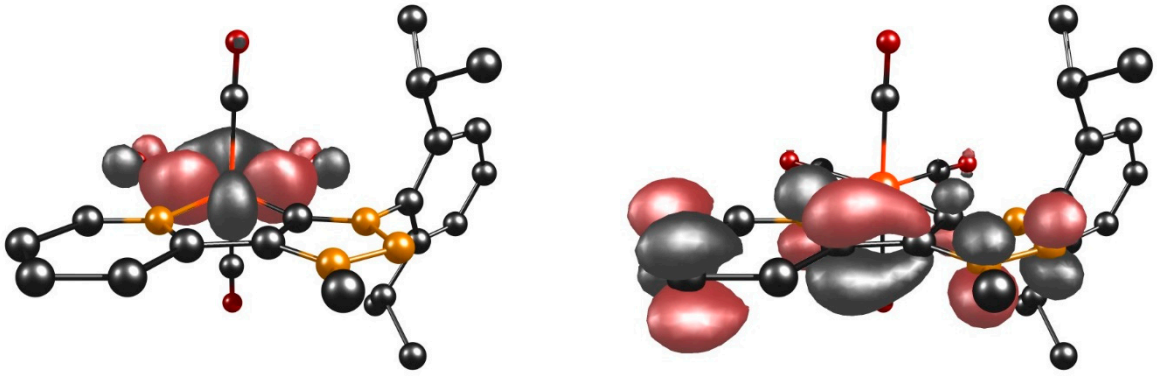

Figure S36. β-HOMO (left) and β-LUMO (right) of complex [W(**C–C**)$(CO)_4]^-$.

Table S17. Energies and compositions of selected orbitals.

MO	Energy / eV
$[\mathbf{W(C-C)(CO)_4}]_{\mathbf{HOMO}}$	−5.0503
$[\mathbf{W(C-C)(CO)_4}]_{\mathbf{LUMO}}$	−2.0464
$[\mathbf{W(C-C)(CO)_4}]^{-}_{\alpha-\mathbf{HOMO}}$	−2.8466
$[\mathbf{W(C-C)(CO)_4}]^{-}_{\alpha-\mathbf{LUMO}}$	−0.9164
$[\mathbf{W(C-C)(CO)_4}]^{-}_{\beta-\mathbf{HOMO}}$	−4.7190
$[\mathbf{W(C-C)(CO)_4}]^{-}_{\beta-\mathbf{LUMO}}$	−1.0525

Table S18. Selected experimental UV/vis data of [W(**C–C**)(CO)$_4$] together with selected TD-DFT calculations.

State	$\lambda_{exp}(\lambda_{DFT})$ / nm	ε / 10^4 M^{-1} cm^{-1}(f)	Main contributing excitation (%)
3	421 (524)	0.51 (0.054)	HOMO–2 → LUMO (86) HOMO–1 → LUMO (8)
9	349 (407)	0.71 (0.013)	HOMO–1→ LUMO+1 (64) HOMO → LUMO+4 (8)
11	349 (398)	0.71 (0.018)	HOMO–2→ LUMO+1 (32) HOMO→ LUMO+3 (36) HOMO→ LUMO+4 (20)
14	304 (336)	1.23 (0.076)	HOMO–2 → LUMO+3 (23) HOMO–1 → LUMO+3 (35) HOMO–1 → LUMO+4 (12)

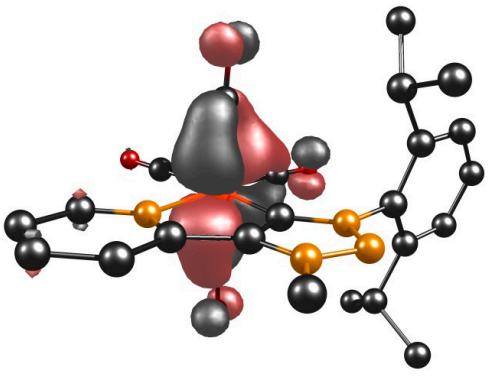

HOMO−2

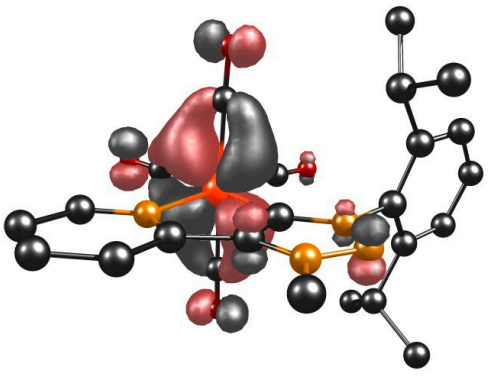

HOMO−1

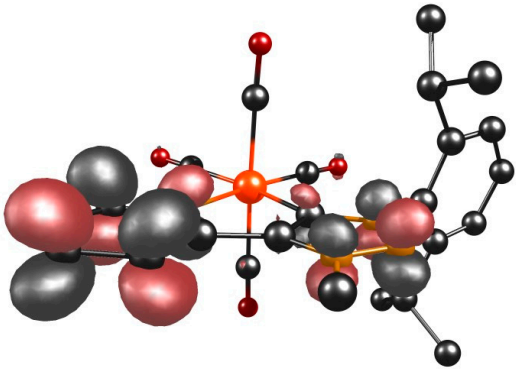

LUMO+1

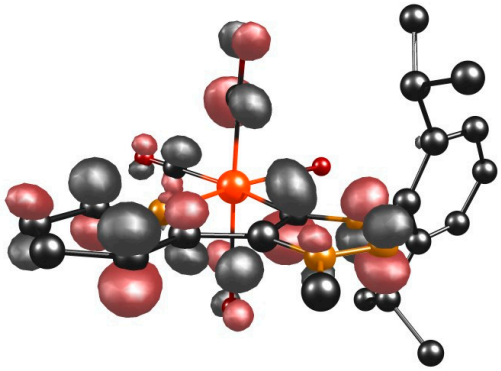

LUMO+3

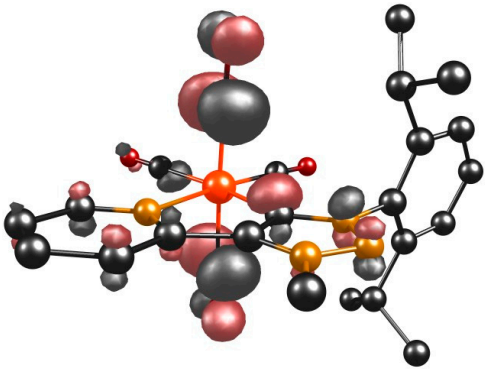

LUMO+4

Figure S37. Involved TD-DFT orbitals of complex [W(**C–C**)$(CO)_4$].

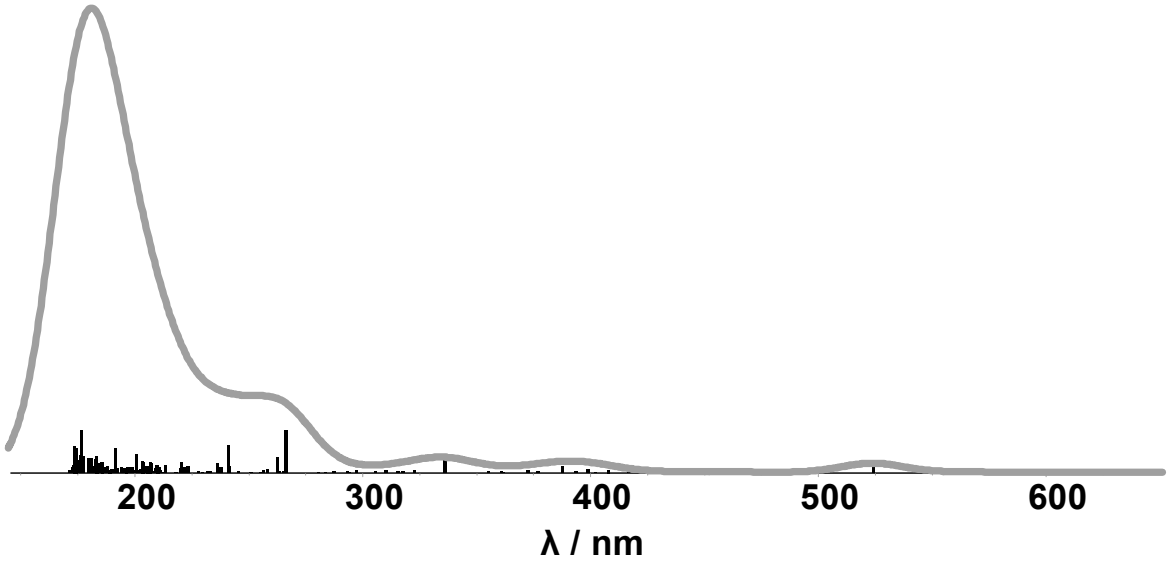

Figure S38. Calculated TD-DFT spectrum with discrete transitions of [W(**C–C**)$(CO)_4$].

Table S19. Selected experimental UV/vis data of [W(**C–C**)(CO)$_4$]$^-$ together with selected TD-DFT calculations.

State	$\lambda_{exp}(\lambda_{DFT})$ / nm	ε / M^{-1} cm^{-1}(f)	Main contributing excitation (%)
1	1583 (1105)	0.08 (0.029)	α-HOMO → α-LUMO (85)
6	1307 (861)	0.13 (0.007)	α-HOMO → α-LUMO+3 (82)
			α-HOMO → α-LUMO+4 (17)
4	905 (761)	0.14 (0.029)	α-HOMO → α-LUMO+2 (59)
			α-HOMO → α-LUMO+4 (21)
12	401 (450)	0.64 (0.005)	α-HOMO−1 → α-LUMO+1 (23)
			α-HOMO−1 → α-LUMO+2 (12)
			β-HOMO → β-LUMO (28)
			β-HOMO → β-LUMO+1 (26)
17	401 (420)	0.64 (0.031)	β-HOMO−2 → β-LUMO (19)
			β-HOMO−1 → β-LUMO (48)
21	401 (399)	0.64 (0.010)	α-HOMO−3 → α-LUMO (24)
			α-HOMO−3 → α-LUMO+1 (13)
			β-HOMO−1 → β-LUMO+2 (17)
26	351 (382)	1.28 (0.011)	α-HOMO−3 → α-LUMO+2 (27)
			α-HOMO−2 → α-LUMO+2 (26)
			β-HOMO−2 → β-LUMO+2 (17)
28	335 (380)	1.45 (0.062)	α-HOMO−3 → α-LUMO (35)
			α-HOMO−2 → α-LUMO+1 (18)
			β-HOMO−2 → β-LUMO (17)

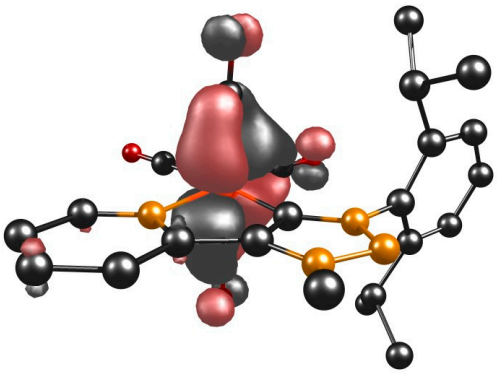

***α*-HOMO–3**

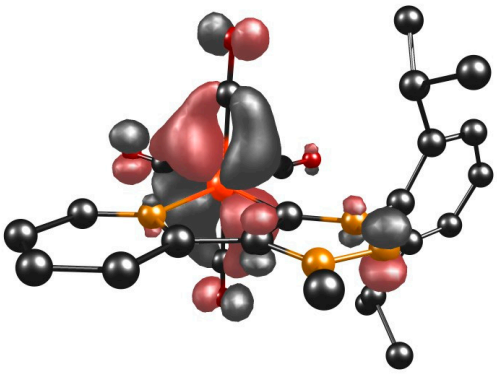

***α*-HOMO–2**

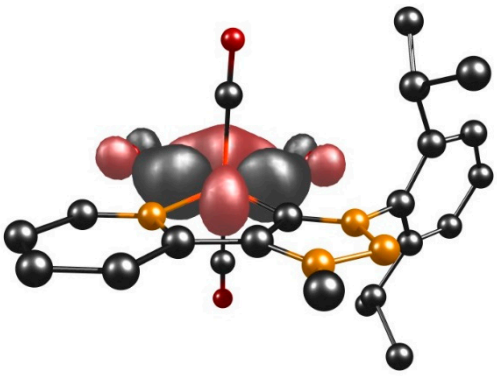

***α*-HOMO–1**

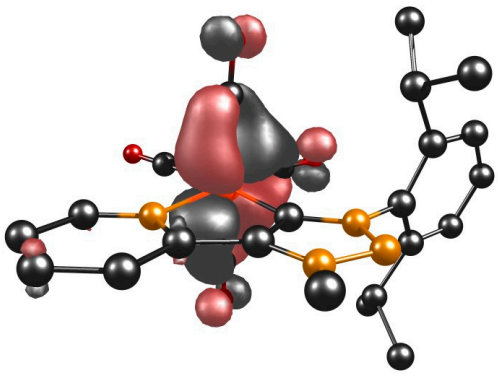

***β*-HOMO–2**

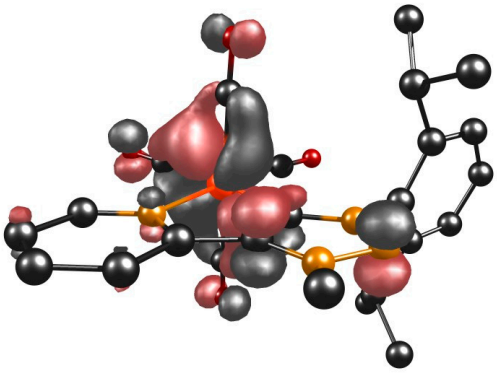

***β*-HOMO–1**

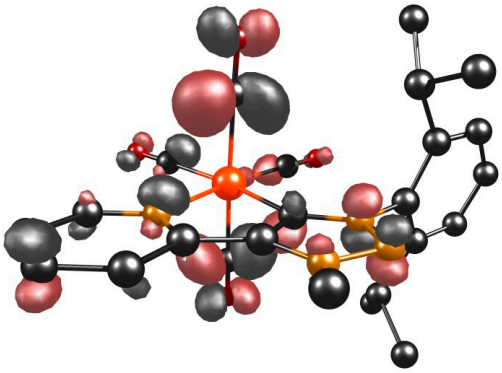

***α*-LUMO+1**

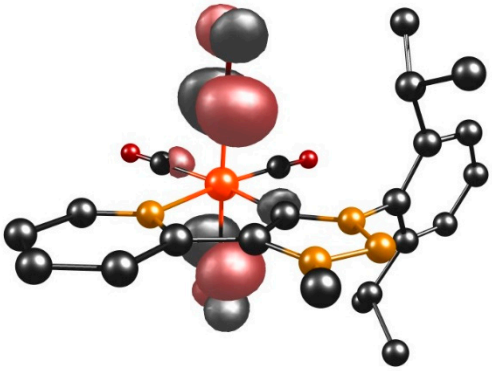

***α*-LUMO+2**

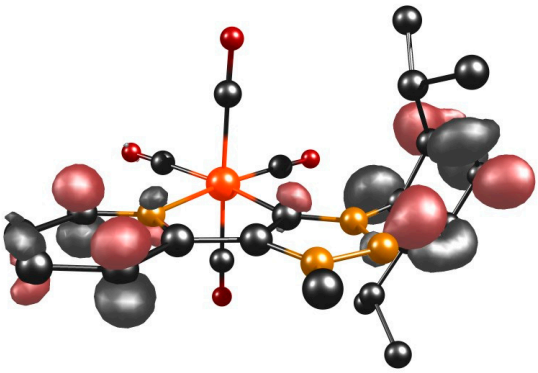

***α*-LUMO+3**

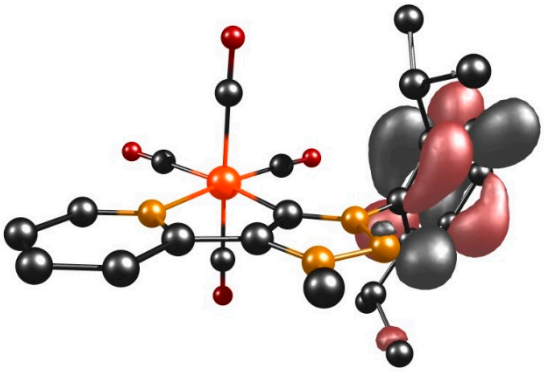

***α*-LUMO+4**

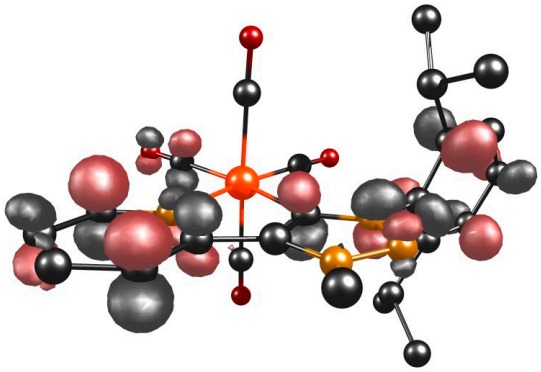

***α*-LUMO+5**

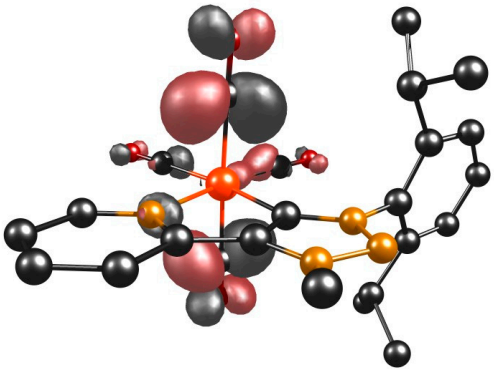

***β*-LUMO+1**

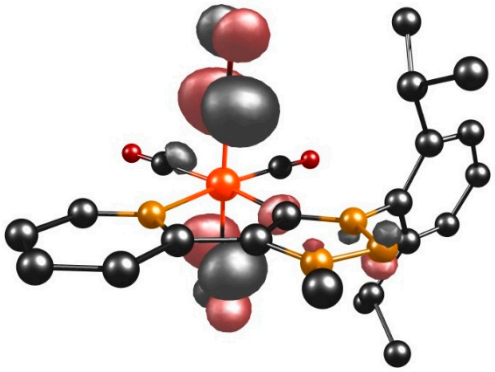

***β*-LUMO+2**

Figure S39. Involved TD-DFT orbitals of complex $[W(\mathbf{C{-}C})(CO)_4]^-$.

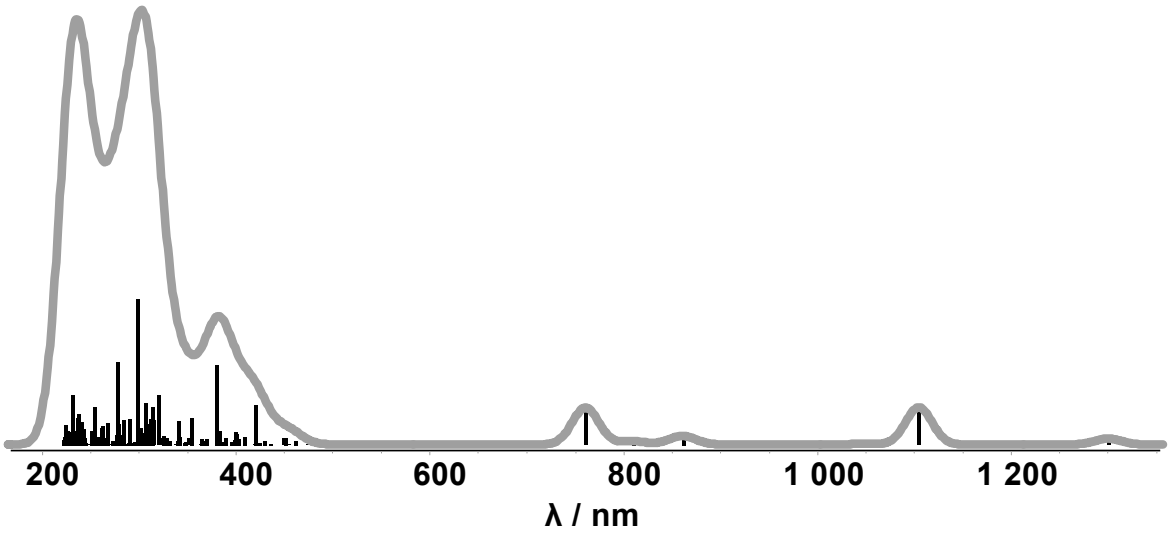

Figure S40. Calculated TD-DFT spectrum with discrete transitions of $[W(\mathbf{C–C})(CO)_4]^-$.

Table S20. Selected MO energies of $[W(\mathbf{C–C})(CO)_4]$ and $[W(\mathbf{C–C})(CO)_4]^-$.

[W(C–C)(CO)$_4$]		**[W(C–C)(CO)$_4$]$^-$**	
MO	**Energy / eV**	**MO**	**Energy / eV**
HOMO–2	−5.3384	***α*-HOMO–3**	−5.0850
HOMO–1	−5.2955	***α*-HOMO–2**	−5.0334
LUMO+1	−1.0686	***α*-HOMO–1**	−4.8048
LUMO+3	−0.8123	***β*-HOMO–2**	−5.0437
LUMO+4	−0.7633	***β*-HOMO–1**	−4.8739
		***α*-LUMO+1**	−0.9098
		***α*-LUMO+2**	−0.6169
		***α*-LUMO+3**	−0.3078
		***α*-LUMO+4**	−0.2644
		***β*-LUMO+1**	−0.9032
		***β*-LUMO+2**	−0.6160

Table S21. XYZ coordinates of optimized [W(**C–C**)$(CO)_4$].

	x	y	z
W	0.93332	4.68088	4.90794
N	-0.35288	3.12918	3.73599
C	2.29383	3.43006	3.71159
C	-0.60342	5.55951	5.84979
C	2.25177	5.86958	5.76133
C	0.76953	6.08591	3.4228
C	1.16495	3.35401	6.45453
C	0.28155	2.23324	2.92699
C	-1.68528	3.05705	3.8414
N	3.6195	3.25206	3.4755
C	1.71557	2.43278	2.9284
O	-1.50776	6.06203	6.38782
O	3.05628	6.56881	6.2367
O	0.69554	6.92453	2.63473
O	1.32595	2.62118	7.32894
C	-0.42303	1.26006	2.22379
C	-2.44662	2.11308	3.17138
H	-2.1511	3.78288	4.49179
N	3.89862	2.26555	2.61765
C	4.7147	3.92498	4.12501
N	2.72628	1.77279	2.29883
H	0.09398	0.55774	1.59025
C	-1.80291	1.19889	2.34806
H	-3.51905	2.09917	3.30479
C	5.12393	5.16957	3.64505
C	5.29619	3.29105	5.23221
C	2.6718	0.62785	1.39841
H	-2.36351	0.44684	1.8095
C	6.21875	5.76269	4.27477
C	4.42875	5.86567	2.49159
C	6.38835	3.92454	5.82182
C	4.73533	1.99556	5.79384
H	2.08111	0.88664	0.52244
H	2.2246	-0.2142	1.92289
H	3.68904	0.38914	1.10587
H	6.5757	6.72405	3.93026
C	6.8545	5.13966	5.33754
H	3.4963	5.339	2.29098
C	4.06656	7.31595	2.83654
C	5.28337	5.79691	1.21852
H	6.87347	3.4715	6.67507
H	3.67292	1.97005	5.54421
C	4.83891	1.92545	7.31881
C	5.38908	0.7541	5.16828
H	7.7051	5.61584	5.8096
H	4.95923	7.91824	3.01601
H	3.44341	7.3668	3.72747
H	3.51544	7.76586	2.00879
H	4.75216	6.25888	0.38329
H	5.51606	4.76399	0.95174
H	6.22642	6.33031	1.35924
H	4.42942	2.82038	7.78935
H	5.87384	1.80636	7.6463
H	4.27856	1.06288	7.68219
H	5.24733	0.72865	4.0884
H	4.94686	-0.14899	5.5946
H	6.46139	0.74011	5.37961

Table S22. XYZ coordinates of optimized $[W(\mathbf{C–C})(CO)_4]^-$.

	x	y	z
W	0.917	4.60166	4.94718
N	-0.34296	3.13651	3.69144
C	2.32321	3.41771	3.7062
C	-0.63944	5.4186	5.90097
C	2.22488	5.74849	5.87516
C	0.76007	6.13548	3.60407
C	1.1327	3.20752	6.43631
C	0.34733	2.25308	2.85166
C	-1.67996	3.05963	3.72821
N	3.64147	3.2736	3.5022
C	1.74608	2.43061	2.88723
O	-1.55852	5.90152	6.44162
O	3.01945	6.43343	6.39525
O	0.6793	7.08169	2.94197
O	1.27647	2.45429	7.29999
C	-0.37882	1.31453	2.074
C	-2.43234	2.16718	2.99085
H	-2.16732	3.76052	4.39388
N	3.9984	2.29046	2.62421
C	4.71616	3.96248	4.15334
N	2.79052	1.78982	2.23478
H	0.15369	0.63345	1.42697
C	-1.74753	1.26887	2.13856
H	-3.50921	2.1621	3.08086
C	5.09367	5.22727	3.68818
C	5.35455	3.32259	5.22235
C	2.78162	0.54771	1.49706
H	-2.29534	0.55071	1.54139
C	6.21655	5.81437	4.26983
C	4.28002	5.94254	2.62561
C	6.47565	3.9477	5.76979
C	4.81064	2.03139	5.80728
H	2.14033	0.6256	0.61995
H	2.43084	-0.27343	2.12894
H	3.79867	0.34133	1.17275
H	6.54801	6.78691	3.93203
C	6.91576	5.16995	5.28221
H	3.24608	5.63416	2.77442
C	4.3199	7.46365	2.7746
C	4.68343	5.52708	1.20295
H	7.00236	3.48057	6.59117
H	3.76273	1.96575	5.51227
C	4.84956	2.04006	7.33713
C	5.51992	0.78721	5.25732
H	7.79018	5.64026	5.7159
H	5.29727	7.87336	2.50945
H	4.08345	7.76852	3.79538
H	3.58393	7.91405	2.10656
H	4.07444	6.06224	0.47095
H	4.539	4.45666	1.04912
H	5.73209	5.77095	1.0114
H	4.36134	2.92886	7.73954
H	5.87352	2.01177	7.71531
H	4.33035	1.16161	7.72404
H	5.40015	0.72572	4.17578
H	5.09192	-0.11286	5.70528
H	6.58648	0.80979	5.49832

S6.40 TD-DFT Calculations of [W(C–N)(CO)$_4$] and [W(C–N)(CO)$_4$]$^-$

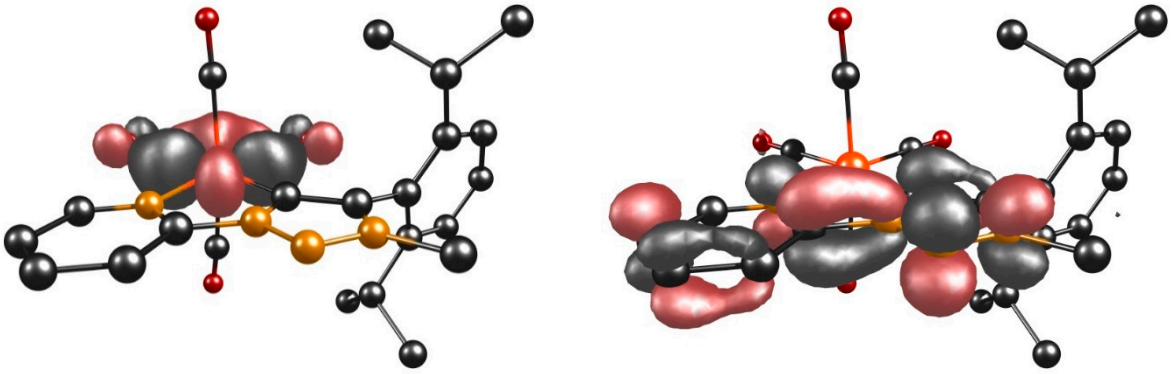

Figure S41. HOMO (left) and LUMO (right) of complex [W(**C–N**)(CO)$_4$].

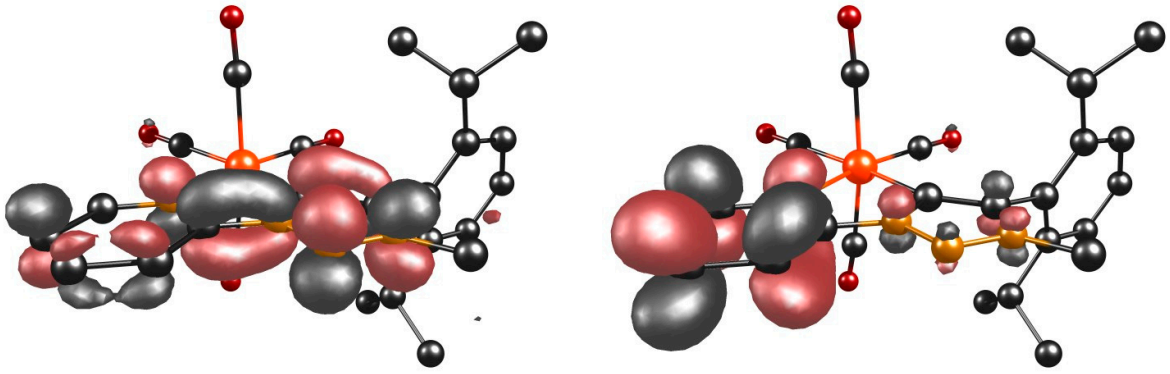

Figure S42. α-HOMO (left) and α-LUMO (right) of complex [W(**C–N**)(CO)$_4$]$^-$.

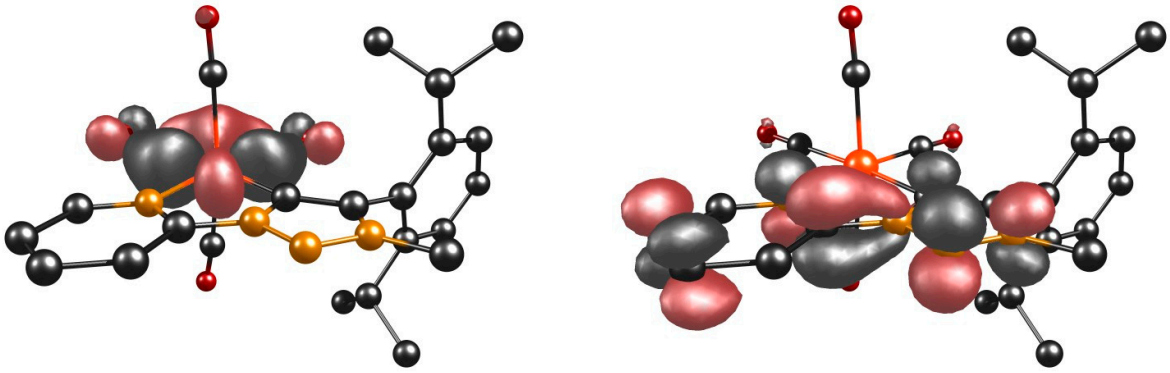

Figure S43. β-HOMO (left) and β-LUMO (right) of complex [W(**C–N**)(CO)$_4$]$^-$.

Table S23. Energies and compositions of selected orbitals.

MO	Energy / eV
$[\mathbf{W(C-N)(CO)_4}]_{\mathbf{HOMO}}$	−5.3143
$[\mathbf{W(C-N)(CO)_4}]_{\mathbf{LUMO}}$	−2.6455
$[\mathbf{W(C-N)(CO)_4}]^{-}_{\alpha\mathbf{-HOMO}}$	−2.9966
$[\mathbf{W(C-N)(CO)_4}]^{-}_{\alpha\mathbf{-LUMO}}$	−0.9720
$[\mathbf{W(C-N)(CO)_4}]^{-}_{\beta\mathbf{-HOMO}}$	−4.8301
$[\mathbf{W(C-N)(CO)_4}]^{-}_{\beta\mathbf{-LUMO}}$	−1.2443

Table S24. Selected experimental UV/vis data of [W(**C–N**)(CO)$_4$] together with selected TD-DFT calculations.

State	$\lambda_{exp}(\lambda_{DFT})$ / nm	ε / 10^4 M^{-1} cm^{-1}(f)	Main contributing excitation (%)
3	447 (534)	0.64 (0.079)	HOMO–2 → LUMO (20) HOMO–1 → LUMO (74)
10	374 (395)	0.51 (0.056)	HOMO–2 → LUMO+1 (47) HOMO → LUMO+3 (43)
9	374 (393)	0.51 (0.035)	HOMO–2 → LUMO+1 (36) HOMO → LUMO+3 (55)
15	301 (318)	0.93 (0.012)	HOMO–1 → LUMO+4 (65)

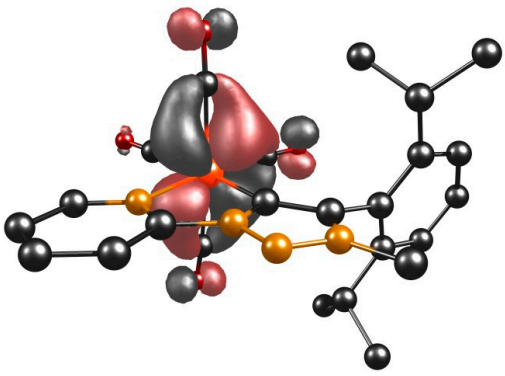

HOMO–2

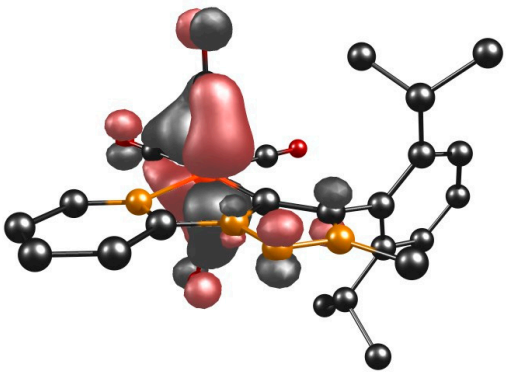

HOMO–1

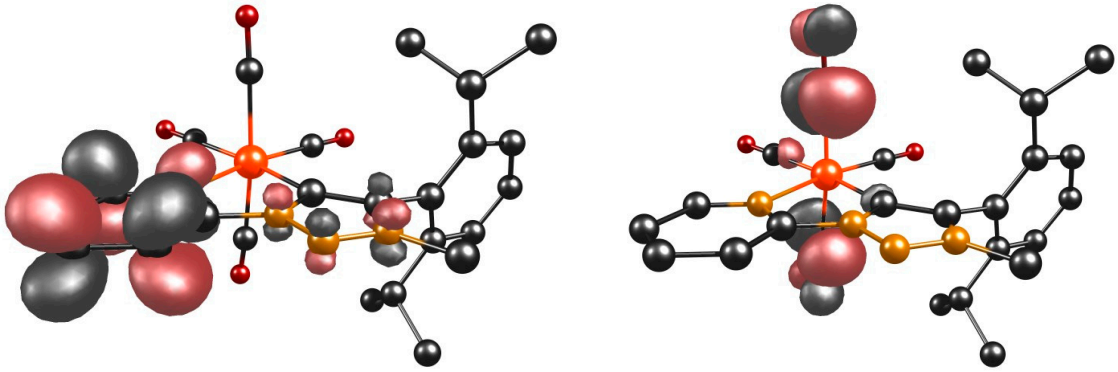

LUMO+1 **LUMO+3**

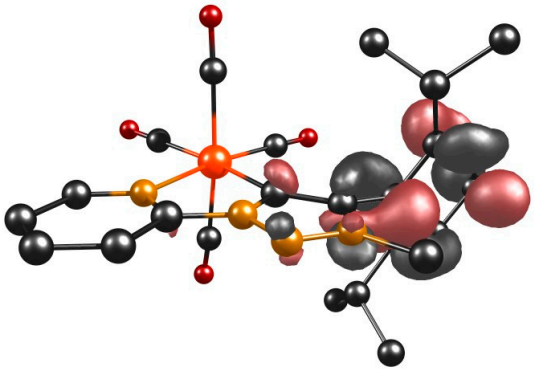

LUMO+4

Figure S44. Involved TD-DFT orbitals of complex [W(**C–N**)(CO)$_4$].

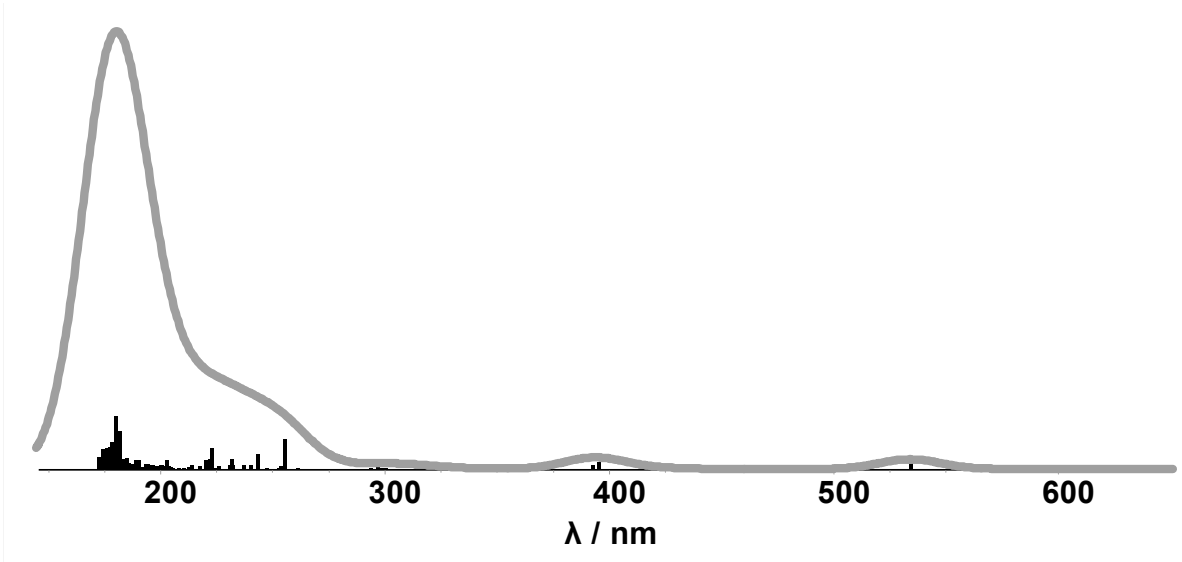

Figure S45. Calculated TD-DFT spectrum with discrete transitions of [W(**C–N**)(CO)$_4$].

Table S25. Selected experimental UV/vis data of [W(**C–N**)(CO)$_4$]$^-$ together with selected TD-DFT calculations.

State	$\lambda_{exp}(\lambda_{DFT})$ / nm	ε / 10^4 M^{-1} cm^{-1}(f)	Main contributing excitation (%)
1	1570 (1242)	0.02 (0.014)	α-HOMO → α-LUMO (96)
3	1185 (927)	0.07 (0.001)	α-HOMO → α-LUMO+1 (99)
4	947 (1022)	0.14 (0.012)	α-HOMO–1 → α-LUMO+2 (98)
5	947 (817)	0.14 (0.006)	α-HOMO → α-LUMO+3 (99)
6	674 (515)	0.56 (0.108)	α-HOMO → α-LUMO+4 (86)
11	622 (454)	0.60 (0.016)	α-HOMO → α-LUMO+6 (47) β-HOMO–1 → β-LUMO+1 (29)
13	575 (448)	0.44 (0.032)	β-HOMO–1 → β-LUMO (68)
17	430 (431)	0.62 (0.015)	β-HOMO–2 → β-LUMO (66)
15	340 (423)	1.55 (0.028)	α-HOMO–1 → α-LUMO+1 (30) β-HOMO → β-LUMO+1 (32)
31	316 (380)	1.90 (0.058)	α-HOMO–3 → α-LUMO (22) β-HOMO–2 → β-LUMO+1 (63)

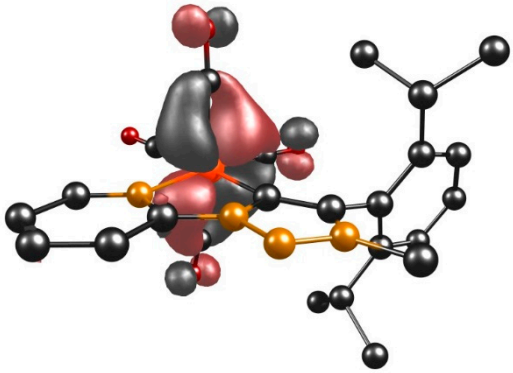

***α*-HOMO–3**

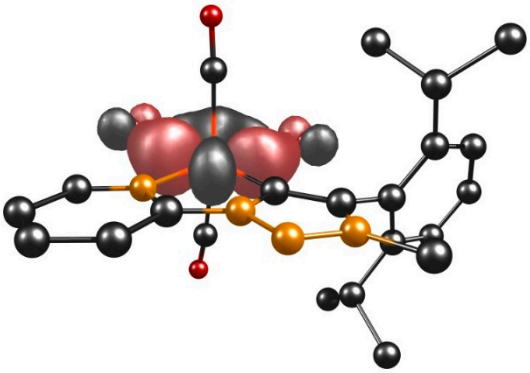

***α*-HOMO–1**

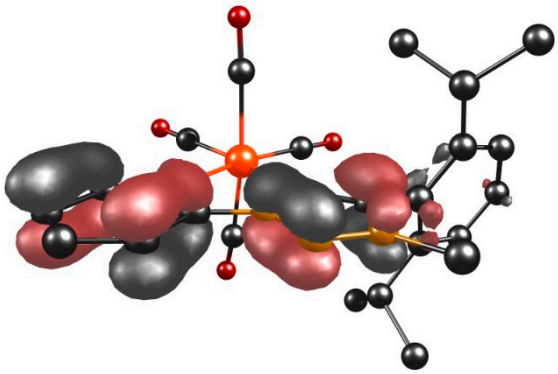

***β*-HOMO–2**

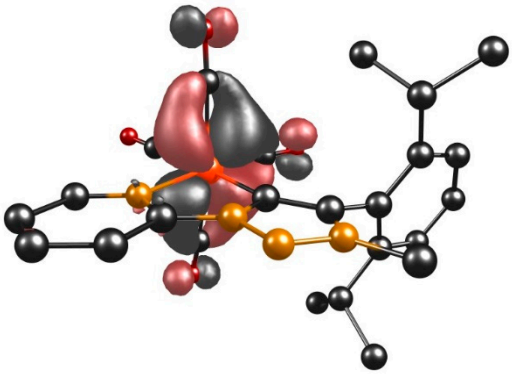

***β*-HOMO–1**

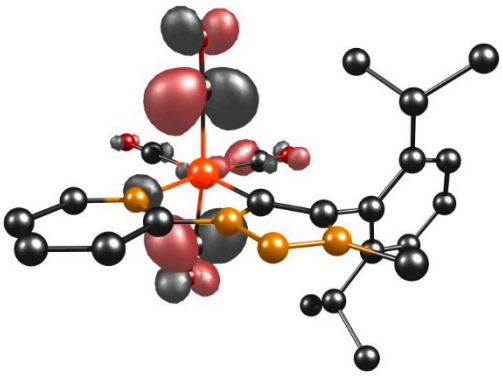

α-LUMO+1

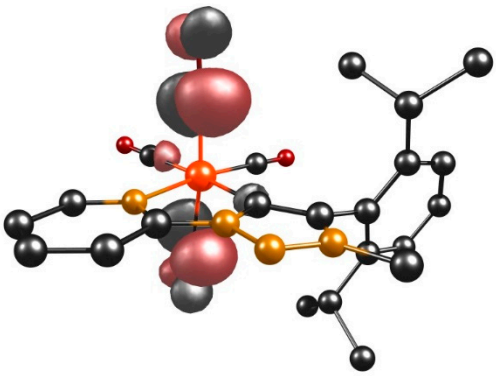

α-LUMO+2

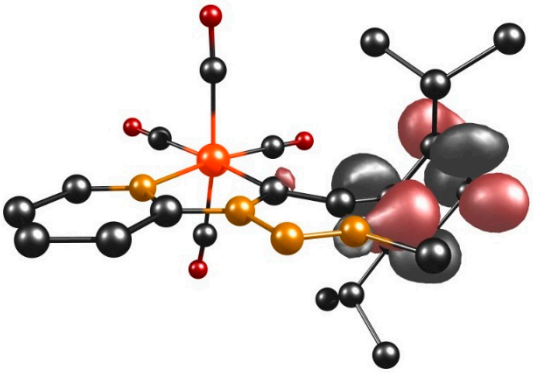

α-LUMO+3

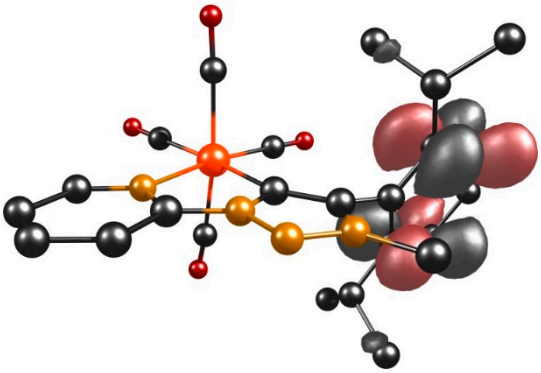

α-LUMO+4

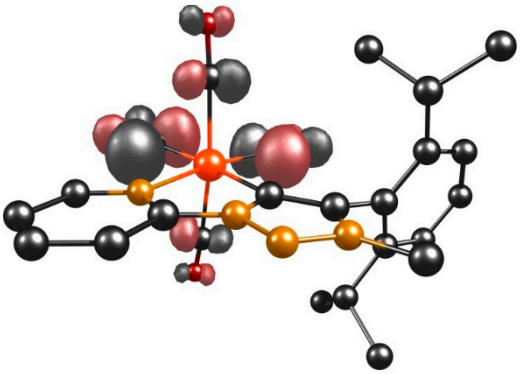

α-LUMO+6

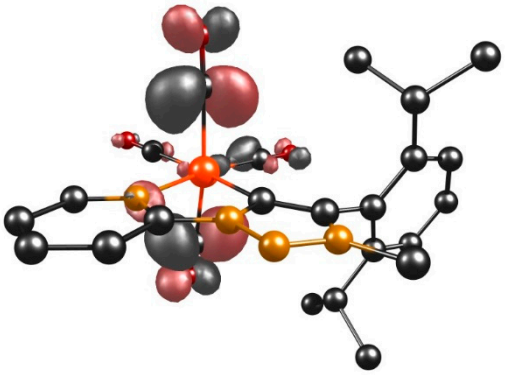

β-LUMO+1

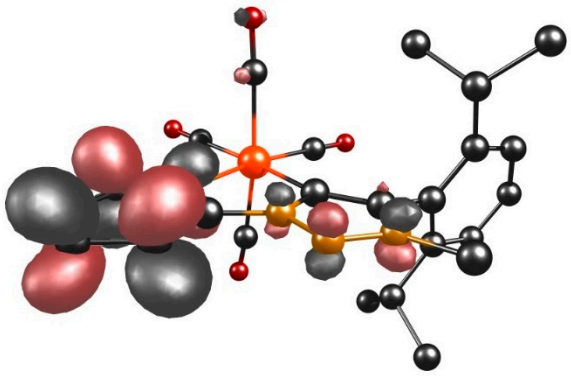

***β*-LUMO+2**

Figure S46. Involved TD-DFT orbitals of complex [W(**C–N**)$(CO)_4$]$^-$.

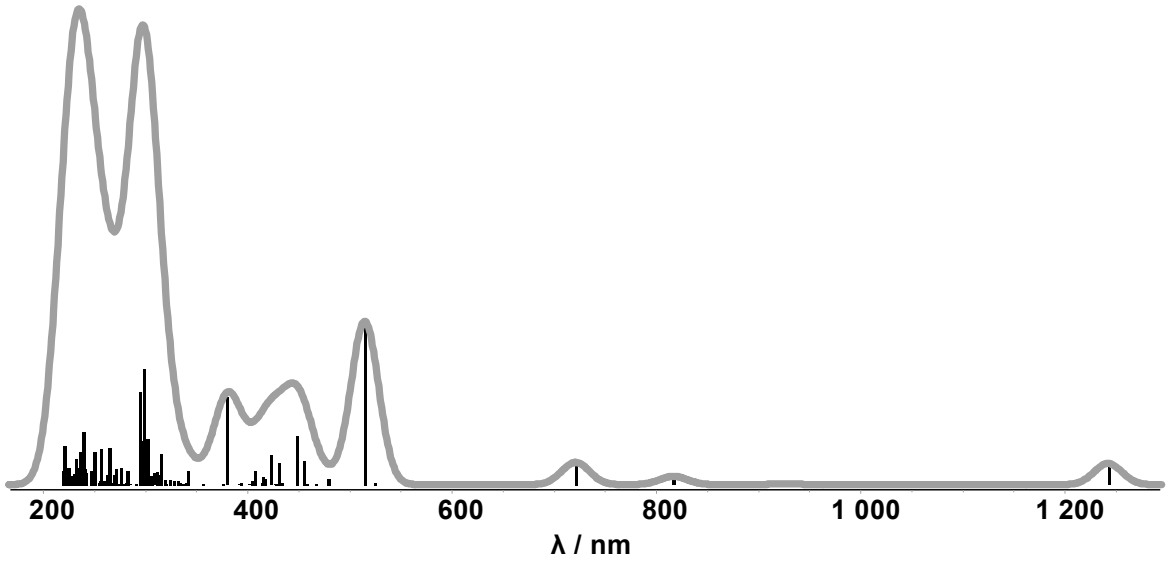

Figure S47. Calculated TD-DFT spectrum with discrete transitions of [W(**C–N**)$(CO)_4$]$^-$.

Table S26. Selected MO energies of [W(**C–N**)(CO)$_4$] and [W(**C–N**)(CO)$_4$]$^-$.

[W(C–N)(CO)$_4$]		**[W(C–N)(CO)$_4$]$^-$**	
MO	**Energy / eV**	**MO**	**Energy / eV**
HOMO–2	−5.4114	***α*-HOMO–3**	− 5.1212
HOMO–1	−5.3226	***α*-HOMO–1**	−4.8312
LUMO+1	−1.5436	***β*-HOMO–2**	−5.0951
LUMO+3	−0.8234	***β*-HOMO–1**	−4.8841
LUMO+4	−0.6371	***α*-LUMO+1**	−0.9098
		***α*-LUMO+2**	−0.6299
		***α*-LUMO+3**	−0.3915
		***α*-LUMO+4**	−0.1097
		***α*-LUMO+6**	0.2604
		***β*-LUMO+1**	−0.9035
		***β*-LUMO+2**	−0.7963

Table S27. XYZ coordinates of optimized [W(**C–N**)(CO)$_4$].

	x	y	z
W	-2.07759	9.73554	9.61697
N	-2.96761	7.65608	10.04448
C	-0.50307	8.2197	9.22942
C	-3.67879	10.84371	10.06891
C	-1.01579	11.32229	9.11795
C	-2.87022	9.7527	7.73163
C	-1.5265	10.04743	11.56671
C	-2.16693	6.58764	9.90972
C	-4.24562	7.43058	10.39694
C	0.80693	8.06144	8.78333
N	-0.86599	6.92263	9.4941
O	-4.61537	11.48775	10.32662
O	-0.36745	12.2394	8.80839
O	-3.39567	9.88172	6.71223
O	-1.28255	10.33587	12.65699
C	-2.57092	5.28107	10.1267
C	-4.74347	6.1598	10.6166
H	-4.86981	8.30563	10.4977
N	1.07888	6.72162	8.8307
C	1.73233	9.07169	8.2307
N	0.0719	6.00309	9.26531
H	-1.87158	4.46832	10.00309
C	-3.89129	5.06731	10.48763
H	-5.78114	6.03457	10.89117
C	2.32432	6.051	8.47017
C	2.79535	9.57707	9.00607
C	1.50774	9.52366	6.91752
H	-4.25204	4.06282	10.66178
H	2.10445	5.24863	7.77093
H	2.78762	5.64725	9.36801
H	2.97747	6.7847	8.0094
C	3.62014	10.54744	8.44257
C	3.00999	9.10062	10.43458
C	2.36207	10.49259	6.39344
C	0.40982	8.93538	6.05046
H	4.44153	10.95367	9.0149
C	3.40765	11.0012	7.14635
H	2.8103	8.02583	10.45686
C	2.00226	9.76379	11.38238
C	4.43763	9.30153	10.9483
H	2.21181	10.84743	5.3825
H	-0.30392	8.43384	6.70358
C	0.99207	7.87157	5.10882
C	-0.36411	9.99906	5.26801
H	4.06438	11.75135	6.72312
H	2.16235	10.84424	11.41442
H	2.11407	9.36649	12.39356
H	0.98043	9.58626	11.05581
H	5.17605	8.86949	10.27082
H	4.5453	8.82094	11.92218
H	4.67254	10.36024	11.0773
H	0.1962	7.39736	4.52941
H	1.51846	7.09405	5.66658
H	1.70213	8.32369	4.41236
H	0.26267	10.48049	4.51497
H	-0.75154	10.77088	5.93338
H	-1.20875	9.53797	4.75346

Table S28. XYZ coordinates of optimized [W(**C–N**)(CO)$_4$]$^-$.

	x	y	z
W	-2.06786	9.72788	9.63463
N	-2.97596	7.67083	10.04528
C	-0.48365	8.21092	9.23315
C	-3.64508	10.84533	10.11098
C	-0.99324	11.30386	9.13403
C	-2.88509	9.76388	7.76288
C	-1.53083	10.02029	11.58842
C	-2.14669	6.58813	9.9007
C	-4.25432	7.43495	10.38142
C	0.79969	8.0526	8.78569
N	-0.88101	6.89132	9.50839
O	-4.56877	11.5093	10.3946
O	-0.33876	12.22052	8.81907
O	-3.43778	9.91139	6.75557
O	-1.31435	10.31458	12.6876
C	-2.59346	5.26842	10.11902
C	-4.77164	6.17214	10.58956
H	-4.87674	8.31371	10.48207
N	1.10927	6.70498	8.80651
C	1.72091	9.06841	8.22967
N	0.08353	5.94564	9.27448
H	-1.90044	4.4488	10.00145
C	-3.90743	5.06597	10.46101
H	-5.812	6.05176	10.85551
C	2.35543	6.05673	8.4784
C	2.78051	9.58273	9.00405
C	1.51676	9.50926	6.90949
H	-4.27689	4.06202	10.6277
H	2.19057	5.27244	7.73759
H	2.80791	5.61295	9.36883
H	3.03014	6.80188	8.06607
C	3.61523	10.54578	8.44067
C	2.98035	9.1201	10.43898
C	2.37823	10.47111	6.38143
C	0.42104	8.92096	6.03996
H	4.43227	10.95543	9.01778
C	3.41849	10.98705	7.13726
H	2.7373	8.05512	10.47279
C	1.99589	9.83107	11.37616
C	4.41474	9.27649	10.94915
H	2.23786	10.81517	5.36469
H	-0.27242	8.39879	6.6979
C	1.00689	7.88611	5.0694
C	-0.37824	9.99061	5.29175
H	4.08171	11.73077	6.71199
H	2.19646	10.90551	11.39812
H	2.08994	9.44178	12.39298
H	0.97196	9.683	11.04179
H	5.1366	8.80672	10.27835
H	4.50764	8.80798	11.93088
H	4.69024	10.32752	11.06085
H	0.21223	7.41289	4.48661
H	1.54693	7.10518	5.60924
H	1.70484	8.35998	4.37434
H	0.23309	10.50368	4.54598
H	-0.77143	10.7368	5.98239
H	-1.22143	9.5309	4.77275

S7. Electrochemical CO_2 Reduction

S7.10 Electrochemical CO_2 Reduction with [Cr(C–C)(CO)$_4$]

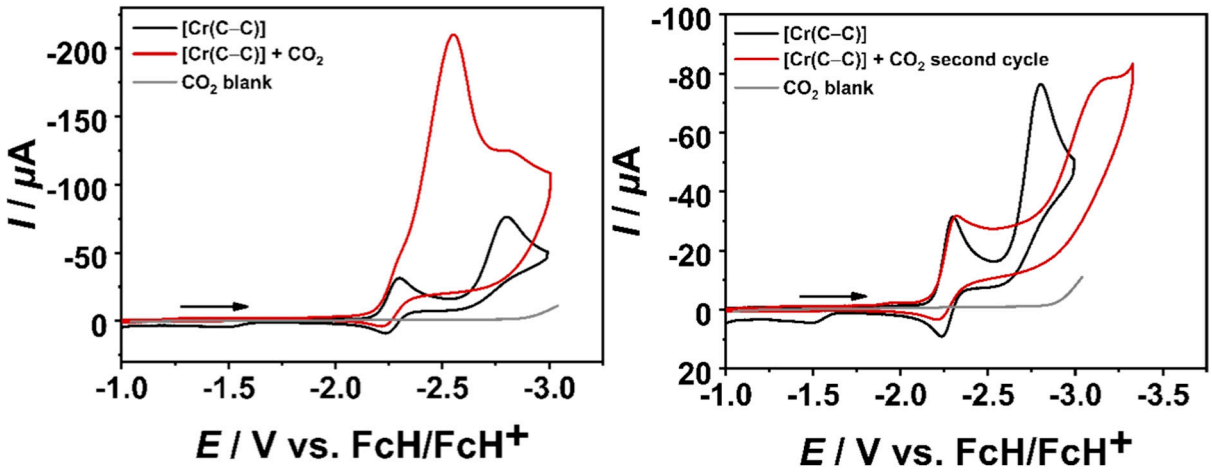

Figure S48. Cyclic voltammograms of [Cr(**C–C**)(CO)$_4$] (1 mM, black) and in the presence of CO_2 (red) at 100 mV/s in CH_3CN/0.1 M Bu_4NPF_6 with a GC working electrode (left: first cycle, right: second cycle).

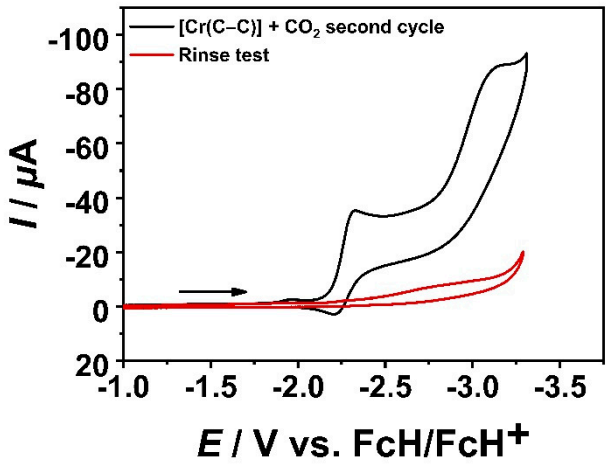

Figure S49. Rinse test of [Cr(**C–C**)(CO)$_4$] (1 mM, black, second cycle) and freshly prepared saturated CO_2 solution (red) at 100 mV/s in CH_3CN/0.1 M Bu_4NPF_6 with a GC working electrode.

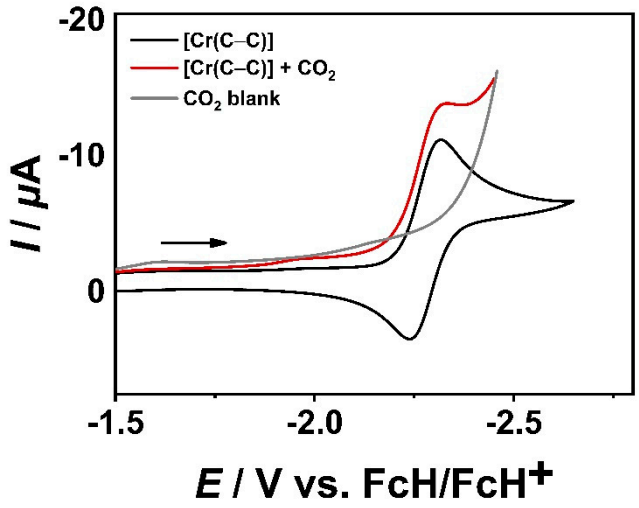

Figure S50. Cyclic voltammograms of [Cr(**C–C**)(CO)$_4$] (1 mM, black) and in the presence of CO_2 (red) at 100 mV/s in CH_3CN/0.1 M Bu_4NPF_6 with a Au working electrode.

S7.20 Electrochemical CO_2 Reduction with [Cr(C–N)(CO)$_4$]

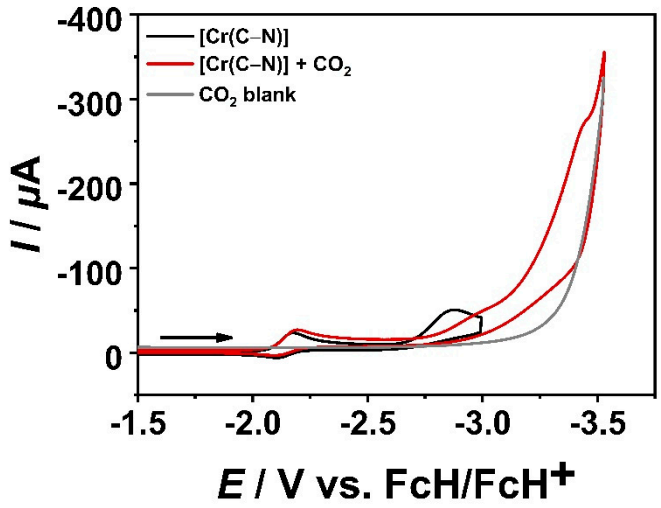

Figure S51. Cyclic voltammograms of [Cr(**C–N**)(CO)$_4$] (1 mM, black) and in the presence of CO_2 (red) at 100 mV/s in CH_3CN/0.1 M Bu_4NPF_6 with a GC working.

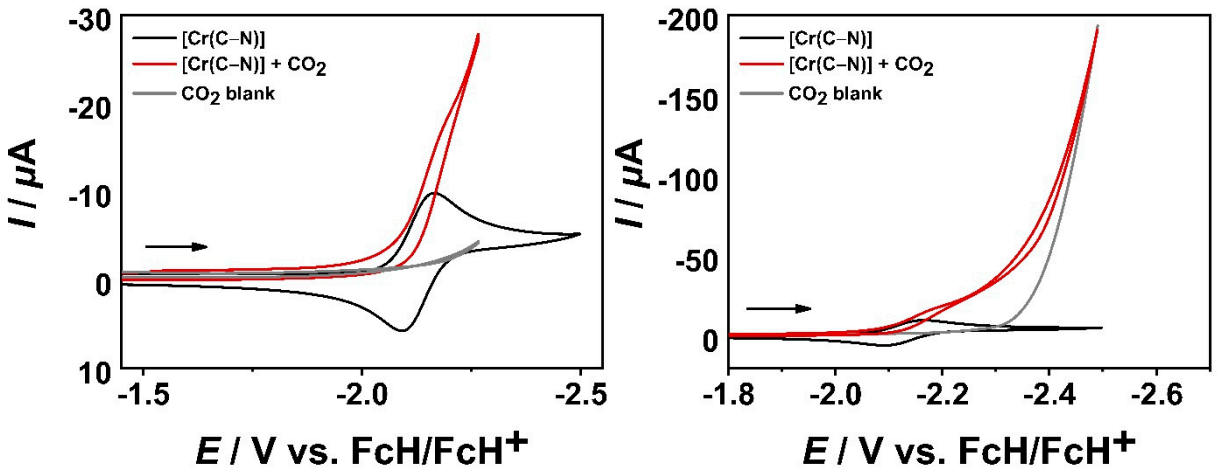

Figure S52. Cyclic voltammograms of [Cr(**C–N**)(CO)$_4$] (1 mM, black) and in the presence of CO_2 (red) at 100 mV/s in CH_3CN/0.1 M Bu_4NPF_6 with a Au working electrode.

S7.30 Electrochemical CO_2 Reduction with [Mo(C–C)(CO)$_4$]

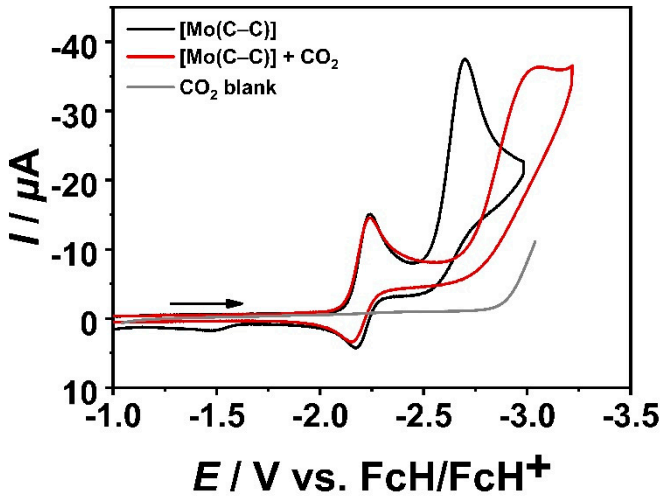

Figure S53. Cyclic voltammograms of [Mo(**C–C**)(CO)$_4$] (1 mM, black) and in the presence of CO_2 (red) at 100 mV/s in CH_3CN/0.1 M Bu_4NPF_6 with a GC working.

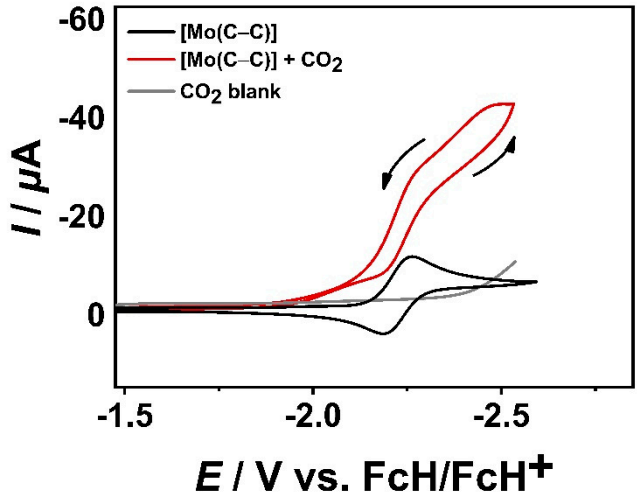

Figure S54. Cyclic voltammograms of [Mo(**C–C**)(CO)$_4$] (1 mM, black) and in the presence of CO_2 (red) at 100 mV/s in CH_3CN/0.1 M Bu_4NPF_6 with a Au working electrode.

S7.40 Electrochemical CO_2 Reduction with [Mo(C–N)(CO)$_4$]

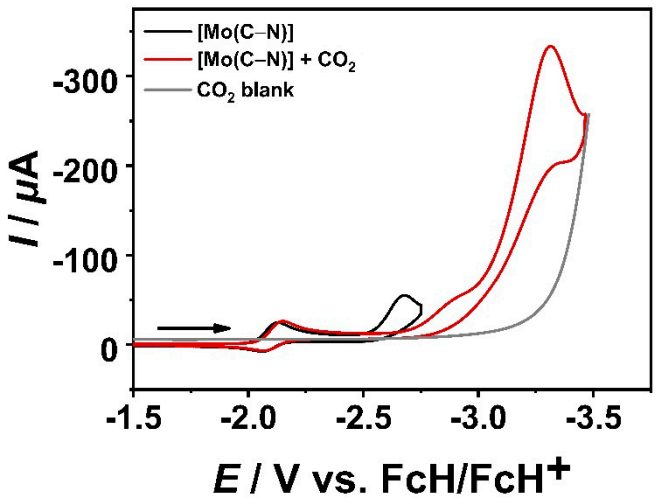

Figure S55. Cyclic voltammograms of [Mo(**C–N**)(CO)$_4$] (1 mM, black) and in the presence of CO_2 (red) at 100 mV/s in CH_3CN/0.1 M Bu_4NPF_6 with a GC working.

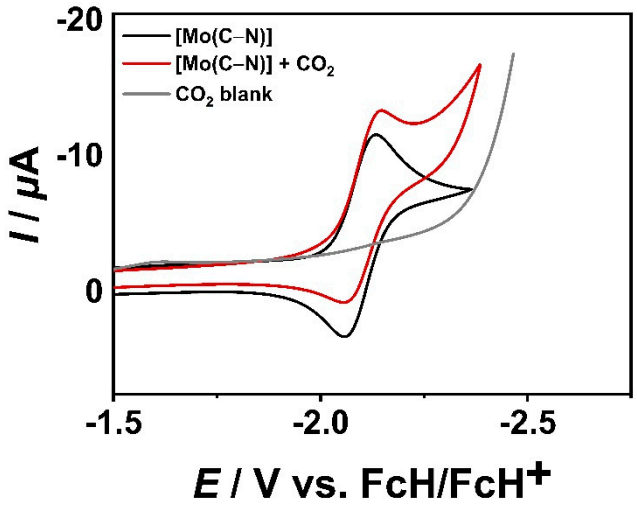

Figure S56. Cyclic voltammograms of [Mo(**C–N**)(CO)$_4$] (1 mM, black) and in the presence of CO_2 (red) at 100 mV/s in CH_3CN/0.1 M Bu_4NPF_6 with a Au working electrode.